Quantifying the three-dimensional stratigraphic expression of cyclic steps by integrating seafloor and deep-water outcrop observations

REBECCA G. ENGLERT* (iD), STEPHEN M. HUBBARD* (iD),
MATTHIEU J. B. CARTIGNY† (iD), MICHAEL A. CLARE‡, DANIEL S. COUTTS* (iD),
SOPHIE HAGE* (iD), JOHN HUGHES CLARKE§ (iD), ZANE JOBE¶ (iD),
D. GWYN LINTERN**, COOPER STACEY** (iD) and DANIELA VENDETTUOLI‡,†† (iD)
*Department of Geoscience, University of Calgary, Calgary, T2N 1N4 AB, Canada (E-mail: rebecca.englert@ucalgary.ca)
†Department of Geography, University of Durham, Durham DH1 3LE, UK
‡National Oceanography Centre, Southampton SO14 3ZH, UK
§Center for Coastal and Ocean Mapping, University of New Hampshire, Durham 03824 NH, USA
¶Chevron Center of Research Excellence, Department of Geology and Geological Engineering, Colorado School of Mines, Golden, 80401, CO, USA
**Natural Resources Canada, Geological Survey of Canada, Sidney, V8L 4B2, BC, Canada
††Ocean and Earth Sciences, University of Southampton, Southampton, SO14 3ZH, UK

Associate Editor – Alexandre Normandeau

ABSTRACT

Deep-water deposits are important archives of Earth's history including the occurrence of powerful flow events and the transfer of large volumes of terrestrial detritus into the world's oceans. However the interpretation of depositional processes and palaeoflow conditions from the deep-water sedimentary record has been limited due to a lack of direct observations from modern depositional systems. Recent seafloor studies have resulted in novel findings, including the presence of upslope-migrating bedforms such as cyclic steps formed by supercritical turbidity currents that produce distinct depositional signatures. This study builds on process to product relationships for cyclic steps using modern and ancient datasets by providing sedimentological and quantitative, three-dimensional architectural analyses of their deposits, which are required for recognition and palaeoflow interpretations of sedimentary structures in the rock record. Repeat-bathymetric surveys from two modern environments (Squamish prodelta, Canada, and Monterey Canyon, USA) were used to examine the stratigraphic evolution connected with relatively small-scale (average 40 to 55 m wavelengths and 1.5 to 3.0 m wave heights) upslope-migrating bedforms interpreted to be cyclic steps within submarine channels and lobes. These results are integrated to interpret a succession of Late Cretaceous Nanaimo Group deep-water slope deposits exposed on Gabriola Island, Canada. Similar deposit dimensions, facies and architecture are observed in all datasets, which span different turbidite-dominated settings (prodelta, upper submarine canyon and deep-water slope) and timescales (days, years or thousands of years). Bedform deposits are typically tens of metres long/wide, <1 m thick and make up successions of low-angle, backstepping trough-shaped lenses composed of massive sands/sandstones. These results support process-based relationships for these deposits, associated with similar cyclic step bedforms formed by turbidity currents with dense basal layers under low-aggradation conditions. Modern to ancient comparisons reveal the

1

stratigraphic expression of globally prevalent, small-scale, sandy upslope-migrating bedforms on the seafloor, which can be applied to enhance palaeoenvironmental interpretations and understand long-term preservation from ancient deep-water deposits.

INTRODUCTION

Submarine canyon–channel-fan systems are important for transferring sediment and other materials (for example, organic carbon, microplastics and other pollutants) from terrestrial to deep marine environments (Normark et al., 1993; Hessler & Fildani, 2019; Kane et al., 2020; Pohl et al., 2020). Their sedimentary deposits store a wealth of information about the Earth's history (for example, climate and tectonic events, Clift, 2006; Castelltort et al., 2017; Daniels et al., 2018; Fildani et al., 2018; Mason et al., 2019), provide a long-term record of turbidity current events required for seafloor hazard assessments (e.g. Goldfinger, 2011; Clare et al., 2015, 2016; Jobe et al., 2018) and host significant natural resources (for example, hydrocarbons, Pettingill & Weimer, 2002). Observations from modern environments are typically a primary source of information about sedimentary processes, which commonly inform interpretations in the rock record. However, modern deep-water environments are notoriously difficult to study due to their location at substantial water depths and distances from the shore, as well as the unpredictable and destructive nature of turbidity currents (Mutti & Normark, 1987; Paull et al., 2003; Sumner & Paull, 2014; Clare et al., 2020). As a result, the understanding of fundamental deep-water sedimentary processes has been limited compared to other depositional environments that are more easily accessed and readily observed on the Earth's surface.

Improved ability to acquire high spatial and temporal resolution marine datasets (e.g. Khripounoff et al., 2003; Xu et al., 2004; Paull et al., 2011; Babonneau et al., 2013; Maier et al., 2013; Hughes Clarke, 2016; Azpiroz-Zabala et al., 2017; Carvajal et al., 2017; Clare et al., 2017; Maier et al., 2019) over the past decade has led to novel insights into turbidity current occurrence and seafloor morphodynamics (Covault et al., 2017; Hage et al., 2018; Mountjoy et al., 2018; Paull et al., 2018; Vendettuoli et al., 2019). In particular, supercritical (i.e. thin and fast) turbidity currents have been shown to form upslope-migrating bedforms (Hughes Clarke, 2016). These features are now commonly recognized on the seafloor and are widely interpreted as upper-flow-regime bedforms (for example, antidunes and cyclic steps), which has resulted in more extensive consideration of supercritical flow in deep-water settings and stratigraphic interpretations (Wynn & Stow, 2002; Fildani et al., 2006; Hofstra et al., 2015; Symons et al., 2016; Lang et al., 2017; Ono & Plink-Björklund, 2017). Seafloor bedforms have been classified into three main groups including large-scale scours, large-scale sediment waves and small-scale sediment waves, although all are sizeable topographic features (>10 m in length; Fig. 1A). They are observed to span a range of dimensions (20 to 7000 m wavelengths, 0.5 to 250 m wave heights), compositions (silt – gravel) and styles (negative relief scours, mixed and positive relief sediment waves), which characterize different components of deep-water systems (for example, canyons, channels, channel–lobe transition zones, lobes and levées) (Fig. 1A and B; e.g. Migeon et al., 2001; Fildani et al., 2006; Lamb et al., 2008; Heiniö & Davies, 2009; Macdonald et al., 2011; Tubau et al., 2015; Zhong et al., 2015; Gardner et al., 2016; Normandeau et al., 2019a; Stacey et al., 2019). As in other sedimentary settings (for example, rivers), bedforms and their deposits could be a reliable tool for deducing deep-water depositional environments and flow conditions (c.f. Allen, 1982; Rubin, 1987; Slootman & Cartigny, 2020). However, there is still uncertainty regarding if and how different types of bedforms observed on the seafloor are expressed in the stratigraphic record, as well as their role in deep-water depositional models (Covault et al., 2017).

Small-scale sediment waves (<300 m wavelength, <8 m wave heights) interpreted to be cyclic steps are evident in many modern sandy submarine channels and lobes (Hughes Clarke,
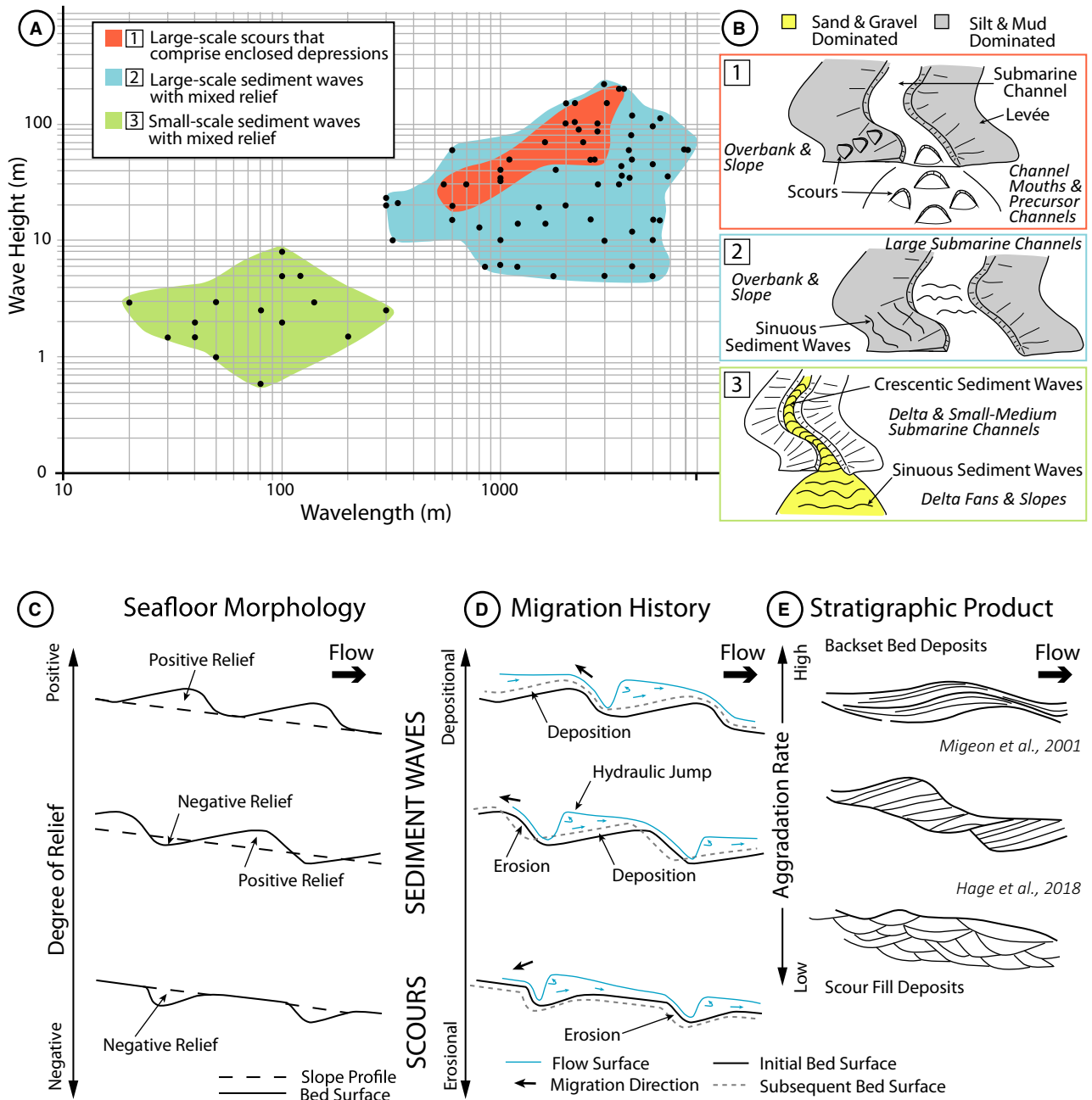
Fig. 1. (A) Graph showing the scale of the three main bedform groups differentiated by Symons *et al.* (2016). (B) Sketches highlighting additional characteristics associated with each bedform group including planform geometry, composition and common location within turbidite-dominated environments. (C) to (E) Linkages between seafloor features, sedimentary processes and stratigraphic products established from observations in modern environments. (C) Morphology of features interpreted to be cyclic steps on the seafloor, often referred to as sediment waves and scours. (D) Flow–seafloor interactions and migration for cyclic step bedforms in (C). (E) Stratigraphic products of these processes based on repeat bathymetry data (Hage *et al.*, 2018) and seismic profiles (Migeon *et al.*, 2001). Parts (A) to (C) adapted from Symons *et al.*, 2016.

2016; Symons *et al.*, 2016; Slootman & Cartigny, 2020). Recent investigations have used repeat bathymetric surveys to link turbidity current morphodynamics, such as bedform migration, to distinct depositional products in modern environments (for example, Squamish prodelta;

Hage *et al.*, 2018; Vendettuoli *et al.*, 2019). Despite recent work, detailed study of deposit geometry and its relation to formative bedform morphology and migration history has not been undertaken. A more comprehensive understanding of three-dimensional architecture is required in order to effectively identify these sedimentary structures in outcrops, which are often oriented oblique to the palaeoflow direction and variably-exposed. In addition, establishing distributions of bedform deposit morphometric properties and how they reflect formative bedforms is needed to support more refined interpretations of palaeoflow information from the rock record.

This study builds on and extends observations from modern environments (Fig. 1) to the interpretation of ancient deep-water deposits. The three-dimensional architecture and nature of sedimentary deposits are examined from upslope-migrating bedforms interpreted as cyclic steps in channelized slopes of the Squamish prodelta (British Columbia, Canada) and Upper Monterey Canyon (California, USA), and findings are compared to a succession of Late Cretaceous Nanaimo Group deep-water slope deposits that crop out on Gabriola Island (British Columbia, Canada). In doing so, ample statistics are produced that quantify bedform deposit scale and geometry as well as describe their 3D shape, distribution and sedimentary features. Collectively these observations directly link deposit characteristics to bedforms formed by naturally-occurring turbidity currents, which is hypothesized to facilitate more robust interpretation of coarse-grained deep-water strata in outcrop. Although differences in spatial and temporal scales make the comparison of modern and ancient datasets difficult, it also means that each holds unique insight into the nature, occurrence and preservation of sedimentary processes on the seafloor. This analysis demonstrates the usefulness of integrating seafloor and stratigraphic datasets, which has proven particularly challenging for deep-water settings in the past (Mutti & Normark, 1987, 1991).

BACKGROUND: STRATIGRAPHIC EXPRESSION OF CYCLIC STEPS

Small-scale sediment waves (<300 m wavelength, <8 m wave height) occur in a wide range of environments including the proximal flanks of volcanic islands, submarine canyon/channels and lobes, and delta channels and slopes (e.g. Casalbore *et al.*, in press; Fildani *et al.*, in press; Piper *et al.*, 1985; Piper & Savoye, 1993; Babonneau *et al.*, 2013; Paull *et al.*, 2013; Mazières *et al.*, 2014; Gales *et al.*, 2019; Normandeau *et al.*, 2019b; Vanderkerhove *et al.*, 2020; Fig. 1A to C). These features are commonly interpreted as long-wavelength upper-flow-regime bedforms called cyclic steps, which are triggered by cyclic step flow instabilities (Cartigny *et al.*, 2011; Symons *et al.*, 2016; Slootman & Cartigny, 2020). Cyclic steps are characterized by a flow configuration where supercritical (Fr > 1) and subcritical (Fr < 1) flow states alternate through internal hydraulic jumps at lee–stoss breaks, in flows that would otherwise be considered supercritical (Fr > 1) throughout (Winterwerp *et al.*, 1992; Parker, 1996; Kostic, 2011; Slootman & Cartigny, 2020; Fig. 1D). Supercritical (more erosive flow) occurs on the lee slope of bedforms while subcritical (more depositional flow) occurs on the stoss slope, resulting in upslope migration.

Several studies have explored the stratigraphic expression and facies that are produced by cyclic step bedforms through the development of conceptual models (Postma & Cartigny, 2014; Postma *et al.*, 2014; Slootman & Cartigny, 2020), numerical models (Kostic & Parker, 2006; Cartigny *et al.*, 2011; Kostic, 2011; Hamilton *et al.*, 2015; Vellinga, *et al.*, 2018), flume experiments (Ono *et al.*, 2019; Postma *et al.*, 2009; Spinewine *et al.*, 2009; Yokokawa *et al.*, 2009; Cartigny *et al.*, 2014; Fedele *et al.*, 2016), and seafloor/shallow subsurface investigations (Migeon *et al.*, 2001; Hage *et al.*, 2018; Vendettuoli *et al.*, 2019). These studies have highlighted end-member depositional architectures and distinct facies related to flow dynamics across cyclic steps. Deposition of massive sands is predicted in the hydraulic jump zone at bedform troughs, while increasingly more stratified deposits are expected towards bedform crests due to flow acceleration (Postma *et al.*, 2009; Postma & Cartigny, 2014). Deposit architectures include backset stratification, formed under high aggradation conditions, and scour fill deposits formed by incomplete preservation under low aggradation conditions (Fig. 1E; Hage *et al.*, 2018; Slootman & Cartigny, 2020). Initial models have largely focused on 2D, flow-parallel perspectives of deposits and often deposition under aggradational conditions (Ono *et al.*, 2019; Cartigny *et al.*, 2014; Postma & Cartigny, 2014; Covault *et al.*, 2017). However, evidence from modern

turbidite systems suggests that many cyclic steps are partially depositional and low-aggradational, which has important implications for both their depositional signature and preservation potential (Hage *et al.*, 2018; Vendettuoli *et al.*, 2019; Slootman & Cartigny, 2020).

Supercritical flow deposits mainly attributed to antidunes, have been previously noted in a limited number of deep-water successions (e.g. Walker, 1967; Skipper, 1971; Mutti & Normark, 1987; Prave & Duke, 1990; Yagishita, 1994; Pickering *et al.*, 2001; Guilocheau *et al.*, 2004). Recent studies have included more frequent identification of a wider spectrum of supercritical-flow bedforms in deep-water deposits (cyclic steps, chutes and pools, antidunes; e.g. Postma *et al.*, 2014, in press; Ito *et al.*, 2014; Bain & Hubbard, 2016; Gong *et al.*, 2017; Ono & Plink-Björklund, 2017; Postma & Kleverlaan, 2018; Cornard & Pickering, 2019; McArthur *et al.*, 2019; Englert *et al.*, 2020), some featuring broad comparisons to seafloor bedform morphology or seismic stratigraphy (e.g. Pemberton *et al.*, 2016; Lang *et al.*, 2017; Brooks *et al.*, 2018; West *et al.*, 2019). This study focuses on detailed quantification of 3D deposit geometry (especially architectures associated with low-aggradation conditions) produced by upslope-migrating bedforms interpreted as cyclic steps in two well-constrained modern environments and applies these findings to a deep-water outcrop.

STUDY AREAS AND DATASETS

Modern: Squamish Prodelta, British Columbia, Canada

The Squamish delta is located within a marine fjord in Howe Sound, British Columbia, and receives more than one million cubic metres of sediment per year from the glacially-influenced Squamish River (Fig. 2A and B; Hickin, 1989). The delta is most active in the summer months due to an influx of seasonal meltwater, during which time >100 flow events may occur with *ca* 20% reaching the base of the prodelta slope (Hughes Clarke *et al.*, 2012b; Clare *et al.*, 2016; Hizzett *et al.*, 2017; Stacey *et al.*, 2019). Events consist dominantly of turbidity currents generated by river plume suspended sediment settling, and occasional subaqueous landslides produced by delta lip failures (Hughes Clark *et al.*, 2014; Clare *et al.*, 2016; Hage *et al.*, 2019). The frequent occurrence of turbidity currents

and position of the system at relatively shallow water depths (spanning 0 to 170 m) makes Squamish an ideal setting for studying turbidity current dynamics and triggers (Hughes Clark *et al.*, 2012a, 2012b, 2014; Clare *et al.*, 2016; Hughes Clarke, 2016; Hizzett *et al.*, 2017; Hage *et al.*, 2019; Stacey *et al.*, 2019).

The Squamish prodelta slope contains three submarine channels (northern, central and southern) that transition into lobes 1 to 2 km from the delta lip (Fig. 2A; Hughes Clark *et al.*, 2014). Active crescentic or sinuous upslope-migrating bedforms are observed within the prodelta channels and lobes, and are interpreted to be supercritical-flow bedforms based on observations of flow–seafloor interactions (Hughes Clarke, 2016), morphodynamic modelling (Covault *et al.*, 2017) and geomorphological characteristics (Hughes Clarke *et al.*, 2012a; Hage *et al.*, 2018; Vendettuoli *et al.*, 2019; Slootman & Cartigny, 2020). Direct monitoring of flows in the northern channel discovered thickening in the high-density basal layer of turbidity currents (i.e. hydraulic jump) at lee–stoss breaks during upslope bedform migration, which is consistent with flow over cyclic steps (Hughes Clarke, 2016). Analysis of time-lapse surveys suggests that sediment is primarily reworked during bedform migration, and thus produces very incomplete successions with a delta-wide average of only 10% stratigraphic preservation after one year (Vendettuoli *et al.*, 2019). Sediment cores and acoustic backscatter images indicate that bedforms in the prodelta channels and lobes dominantly consist of coarse-grained sand (Hughes Clarke *et al.*, 2012a; Hage *et al.*, 2018; Stacey *et al.*, 2019).

In 2011, multibeam bathymetric surveys of the entire Squamish prodelta (93 surveys in total) were collected every weekday over four months in the summer (Fig. 2E; Hughes Clark *et al.*, 2012a, 2012b, 2014). The spatial (0.1 m vertical, 2 × 2 m grid pixels) and temporal (every one to three days) resolution of the surveys allows seafloor changes resulting from almost daily turbidity currents to be captured in an extremely high level of detail (c.f. Hizzett *et al.*, 2017; Hage *et al.*, 2018). A subset of this dataset (12 surveys in total) covering the lower southern channel, channel-lobe transition zone and lobe was used in this study, including surveys that preceded and followed the seven flow events in the southern channel that extended to the lobe at the base of the prodelta slope (Fig. 2E; Clare *et al.*, 2016). Difference maps
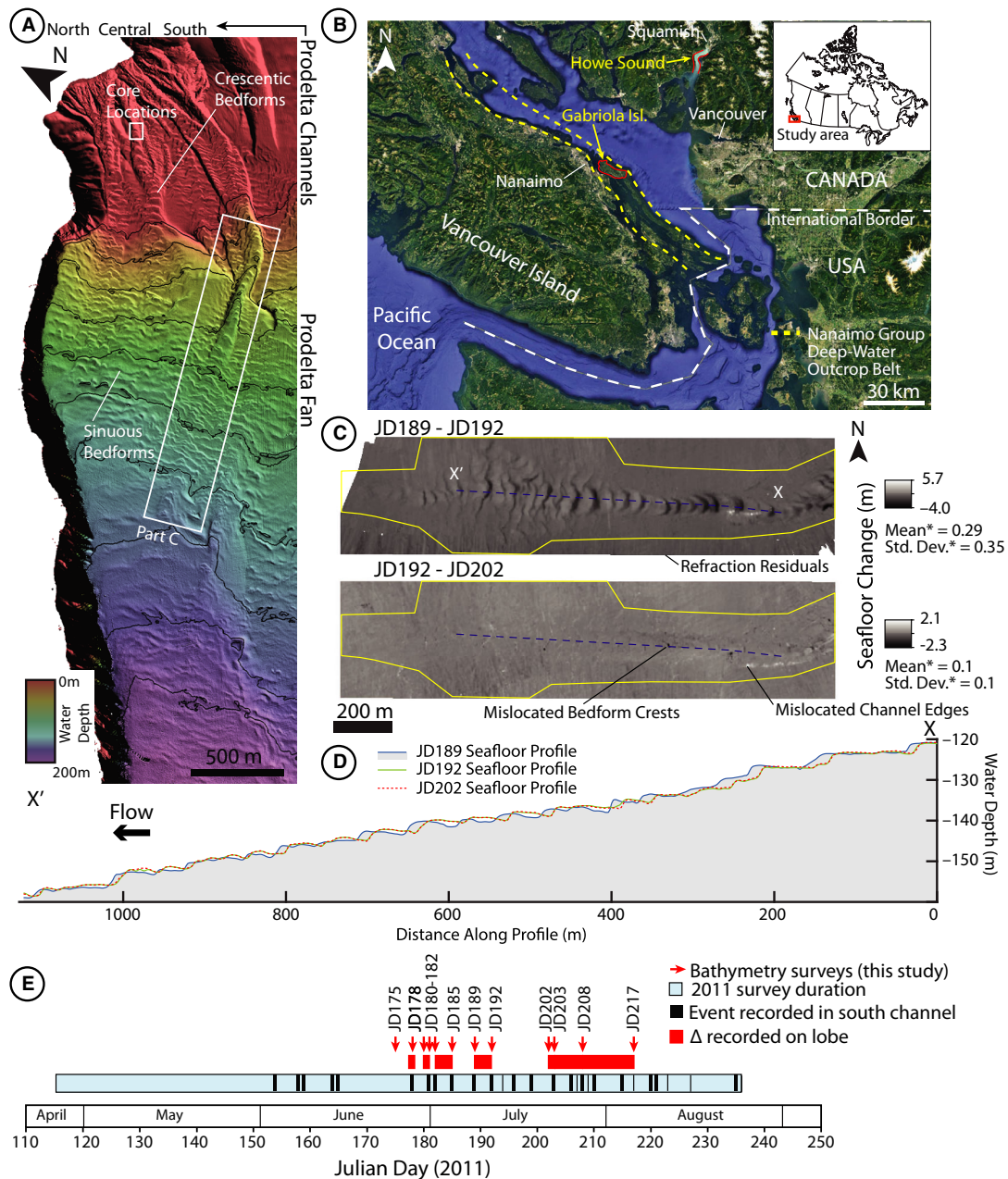
Fig. 2. Squamish prodelta study area. (A) Bathymetry map with white boxes indicating the location of sediment cores (Hage *et al.*, 2018) and repeat bathymetric datasets (Hughes Clark *et al.*, 2014) used in this study. (B) The location of modern (Howe Sound) and ancient (Gabriola Island) study areas on the south-west coast of Canada. The upper fjord and island within the Nanaimo Group outcrop belt are outlined in red. (C) Seafloor difference maps for the lower southern prodelta channel and fan – see location in (A). The upper map shows seafloor changes associated with a turbidity current event. The lower map was created over a time period in which no turbidity current events occurred, where minor seafloor changes reflect errors associated with data acquisition and positioning. Mean and standard deviation seafloor change (* – statistics for absolute magnitude of change) was calculated for each map over the area delineated by the yellow polygons, which encompasses the southern channel and lobe. (D) Seafloor profiles along bedforms in the southern channel thalweg from bathymetric surveys used to produce the difference maps shown in (B) and (C) (profile location indicated by blue-dashed line). (E) Timing of repeat bathymetry survey acquisition and turbidity current events/seafloor changes recorded in the southern channel and lobe over summer, 2011. Red arrows mark the timing of bathymetry surveys used in this study, which precede and follow turbidity current events that reached the base of the prodelta (adapted from Clare *et al.*, 2016). See Appendix S2 for all seafloor difference maps and profiles between turbidity current events in the investigated area.

created between surveys where flow events occurred document a distinct alternating pattern of erosion (up to 5.5 m) and deposition (up to 6 m) within the channel and lobe associated with bedform migration (Fig. 2C and D; c.f. Hughes Clark *et al.*, 2012a, 2014; Hage *et al.*, 2018; Vendettuoli *et al.*, 2019). On the other hand, overall minimal seafloor change (average magnitude of 0.14 m) over the channel and lobe is recorded in difference maps created between surveys not affected by flow events (Fig. 2C and D; see Appendix S1 for table comparing the magnitude of seafloor changes between surveys). Error ranges established for a larger portion of the 2011 Squamish prodelta bathymetry dataset also revealed small seafloor changes, 4 cm ± 23 cm, in the absence of turbidity current events (Hizzett *et al.*, 2017; Vendettuoli *et al.*, 2019). Local outlier differences (up to 5.2 m) between these surveys appear to relate to minor positioning errors, which result in the slight offset of channel margins or bedform crests, or refraction residuals at the edge of swaths along the perimeter of the datasets (Fig. 2C; Hughes Clarke *et al.*, 2012a). In addition to bathymetric surveys, sediment cores obtained from the central channel in 2016 (Hage *et al.*, 2018) were used to capture the sedimentological characteristics of bedform deposits on the channelized slope (Fig. 2A).

Modern: Upper Monterey Canyon, California, USA

The Monterey Canyon is a large submarine canyon–channel system incised into the shelf in Monterey Bay, which extends for >400 km onto the Monterey fan off the west coast of California (Fig. 3A; Normark, 1970; Greene, 1977). An estimated 200 000 to 500 000 m^3 of sediment per year is delivered to the canyon head by littoral transport sourced from nearby rivers and coastal erosion (Best & Griggs, 1991; Eittreim *et al.*, 2002). Several processes are responsible for sediment transport in the Monterey Canyon including: sediment gravity flows and other forms of mass movement, which are capable of delivering and transporting mixed sediment loads of up to gravel-sized particles (Xu *et al.*, 2004; Paull *et al.*, 2018); and internal tides, which can re-suspend and re-distribute fine-grained material (Xu & Noble, 2009; Maier *et al.*, 2019b). Turbidity currents with varying runout distances have been documented to occur sub-annually (Xu *et al.*, 2004; Paull *et al.*, 2010, 2018; Symons

et al., 2017; Heerema *et al.*, 2020) but rarely reach the Monterey fan (Stevens *et al.*, 2014). Like the Squamish delta, the Monterey Canyon has been an important site for studying deep-water sediment transport processes and for developing sophisticated seafloor mapping and active flow monitoring technologies (e.g. Paull *et al.*, 2003, 2010, 2018; Xu *et al.*, 2004, 2008; Smith *et al.*, 2005, 2007; Symons *et al.*, 2017; Maier *et al.*, 2019a).

The upper Monterey Canyon, located between 20 m and 200 m water depths, consists of four tributary heads that converge to a sinuous axial channel (Fig. 3B). The active tributaries and main channel contain upslope-migrating bedforms, which have been interpreted as cyclic steps based on their geometry and migration history (Cartigny *et al.*, 2011; Kostic, 2011; Symons *et al.*, 2016). Cores and samples from bedforms on the axial channel floor consist of gravel and sand (Paull *et al.*, 2005,2010,2011; Maier *et al.*, 2019).

Between September 2002 and March 2014 multibeam bathymetric surveys of the Upper Monterey Canyon were conducted almost annually – biannually by the Seafloor Mapping Lab at California State University, Monterey Bay, with similar spatial resolution to Squamish datasets (*ca* 0.2 m vertical resolution, 3 × 3 m grid pixels). These data can be freely downloaded from the California Seafloor Mapping Project (http://seafloor.otterlabs.org). Select bathymetric surveys within the Monterey dataset have been previously used to investigate geomorphic changes and sediment transport (2002 to March 2003 surveys in Smith *et al.*, 2005; 2002 to February 2005 surveys in Smith *et al.*, 2007), and bedform migration (2002 to February 2006 surveys in Xu *et al.*, 2008; 2002 to March 2005 surveys in Cartigny *et al.*, 2011) within the Upper Monterey Canyon. Fourteen of the surveys with sufficient coverage and resolution, spaced 76 to 918 days apart were used in this study (Fig. 3D). Flow events in the Monterey Canyon are less frequent and not as well-constrained between acquisition periods as on the Squamish prodelta. Seafloor changes between each survey indicate the occurrence of at least one flow event; however, they likely reflect the combined effect of multiple events as monitoring programs in the upper Monterey canyon typically record between three and eight flows per year (Xu *et al.*, 2004; Paull *et al.*, 2010, 2018). On difference maps, considerable seafloor changes are observed at the canyon head and within the axial channel related
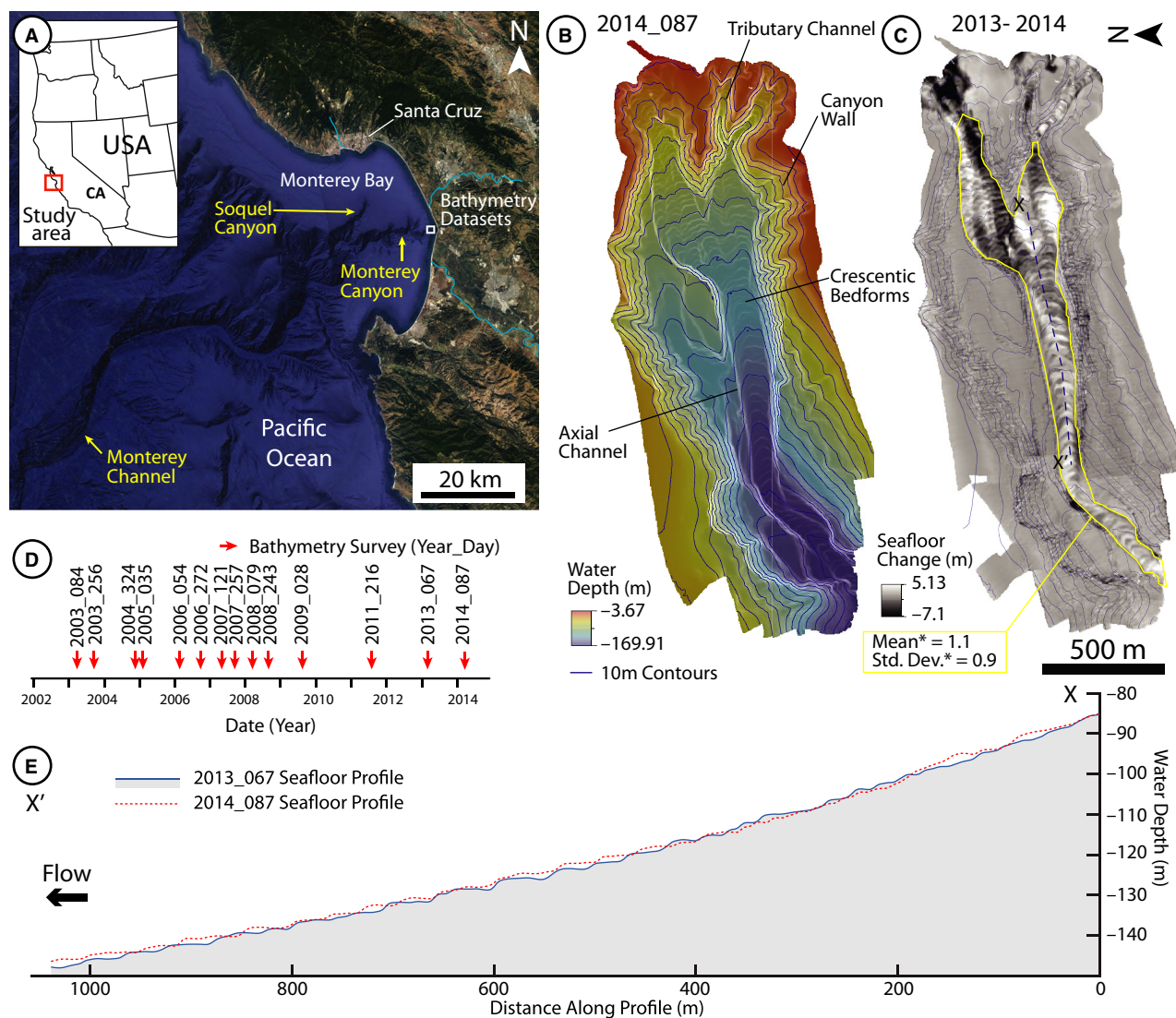
Fig. 3. Monterey Canyon study area. (A) Location in Monterey Bay on the west coast of California. The extent of the repeat bathymetry dataset in the uppermost canyon is shown. (B) Bathymetry map of the upper Monterey Canyon with key morphological features labelled. (C) Seafloor difference map between 2013 and 2014 bathymetry surveys. Significant erosion and deposition is observed at the canyon head and within the axial channel, outlined in yellow, while minimal seafloor changes occur on the canyon flanks (* – statistics for absolute magnitude of change). (D) Acquisition timing of bathymetric surveys used in this study (datasets from the Seafloor Mapping Lab of the California State University Monterey Bay). (E) Seafloor profiles along bedforms in the channel thalweg from bathymetric surveys used to produce the difference map shown in (C) (profile location indicated by the blue-dashed line). See Appendix S3 for all seafloor difference maps and profiles between bathymetric surveys in the investigated area.

to bedform migration (average magnitude of 1 m, up to 11 m), while minimal changes are observed on the canyon flanks (average magnitude of 0.14 m, up to 1.5 m) where presumably no or minor turbidity currents occur (Fig. 3C and E; see Appendix S1 for table comparing the magnitude and distribution of seafloor changes between surveys).

Ancient: Twin Beaches Peninsula, Gabriola Island, British Columbia, Canada

The Nanaimo Group is an up to 4 km thick succession of Late Cretaceous forearc basin fill deposits, presently exposed in the Cowichen fold and thrust belt in south-western British Columbia (Fig. 2A; Mustard, 1994). Its upper
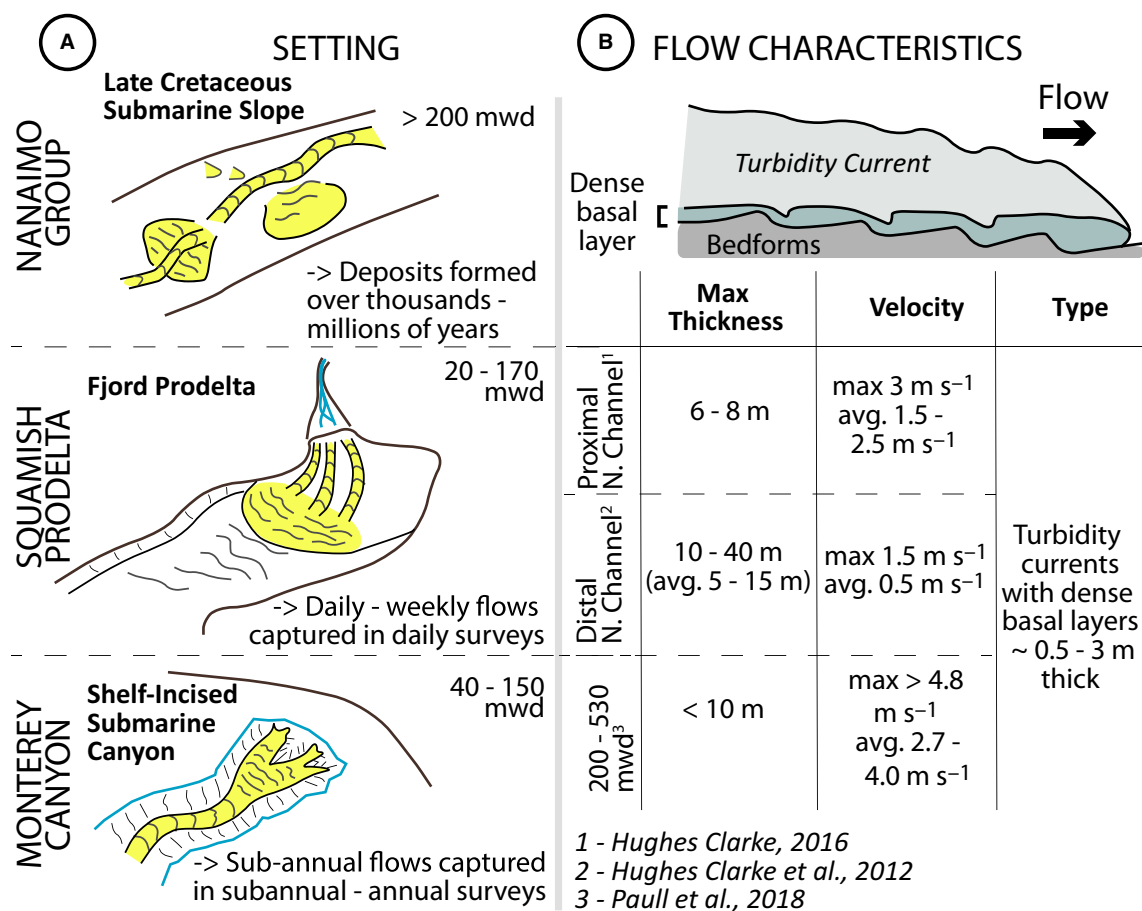
units consist of deep-water strata and make up the bedrock of the Gulf Islands in the Strait of Georgia (Figs 2B and 4B; England & Hiscott, 1992; Katnick & Mustard, 2003). Coarse-grained sandstone and conglomerate-prone deposits form the resistant cores of individual islands, which alternate with and laterally transition to fine-grained lithologies (Bain & Hubbard, 2016; Englert *et al.*, 2018). The area of interest for this study is a succession of the Gabriola Formation exposed in the intertidal zone around the Twin Beaches Peninsula at the north-west end of Gabriola Island (Figs 2B and 4B).

On Gabriola Island, upper Nanaimo Group units are exposed in a north-west plunging syncline (Fig. 4B). The Gabriola Formation consists of thick-bedded, coarse-grained sandstone with packages of interbedded very fine-grained sandstone and siltstone, interpreted to be largely deposited within or in association with submarine channels (England & Hiscott, 1992). Foraminifera from fine-grained intervals within the formation on Gabriola Island indicate palaeo-water depths between 600 m and 1200 m (England & Hiscott, 1992). Palaeoflow measurements around the island range from south-west to north-east but are dominantly west/north-west, generally parallel to the orientation of the island (Fig. 4B).

METHODS

To characterize the stratigraphic products of upslope-migrating bedforms, this study integrates and compares observations of deposit geometry, architecture and facies from different marine settings (delta slope, proximal canyon and deep-water slope) over different temporal periods (daily, yearly, geological timescales; Fig. 5A).

Seafloor observations

Water depth values were extracted from each survey in the Squamish prodelta and Upper Monterey Canyon datasets along dip, oblique (45°) and strike-oriented profiles (Fig. 8A). Subsequent surveys were stacked to determine areas of erosion and deposition, and ultimately reconstruct the depositional products associated with upslope bedform migration (Fig. 6, Appendix S4). Bedform morphology (wavelength, wave height, lee and stoss slope angles), migration history (magnitude and direction) and stratigraphic evolution (amount of deposition and erosion/reworking) were determined for each time step in dip-oriented profiles in order to capture the nature of seafloor features and sediment transport (Fig. 6).

Fig. 4. Twin Beaches Peninsula study area (broader location and Nanaimo Group outcrop belt in Fig. 2B). (A) Nanaimo Group stratigraphic chart (modified from Matthews *et al.*, 2017). (B) Geological map of Gabriola Island including Nanaimo Group stratigraphy, structural features and palaeoflow measurements for the Gabriola Formation. Colours correspond to the formations in (A).

Fig. 5. (A) Comparison of turbidite-dominated settings for modern and ancient study areas. The approximate depth (mwd – mean water depth) and timescale encompassed by each dataset is also indicated. (B) Comparison of flow characteristics (thickness, velocity and type) observed within the study areas but outside the investigated datasets. These observations come from previous monitoring studies of the northern channel on the Squamish Delta (shown in Fig. 2A) and further downslope in the Monterey Canyon using suspended instrument packages such as acoustic Doppler column profilers and imaging multibeams.

The geometry (length and maximum thickness) and architecture of resulting deposits was then qualitatively and quantitatively evaluated in a variety of orientations (for example, dip, oblique and strike) relative to the flow direction (Figs 6 and 8A). Localized erosion and deposition observed in areas or time periods unaffected by turbidity currents likely reflects the presence of some artificial seafloor changes in stratigraphic reconstructions due to systematic surveying and/or positioning errors (Figs 2C and 3C; Hughes Clarke *et al.*, 2012a). However, these changes are small compared to those associated with actual flow events (Appendix S1). Upslope-migrating bedforms have been previously described in the Squamish (Hughes Clark *et al.*, 2012a, 2012b, 2014; Clare *et al.*, 2016;

Hizzett *et al.*, 2017; Vendettuoli *et al.*, 2019) and Monterey datasets (Smith *et al.*, 2005, 2007; Cartigny *et al.*, 2011) used here, and stratigraphic reconstructions have been made along bedforms in the Squamish prodelta southern channel (Vendettuoli *et al.*, 2019). This study supports the observations from these initial investigations and provides new results including more detailed analysis of bedform morphology, migration and associated deposit geometries in three-dimensions, and the generation of large quantitative datasets along variably oriented cross-sectional profiles.

The sedimentological characteristics of bedform deposits were captured in seven piston cores from the Squamish prodelta, previously photographed and described by Hage *et al.*
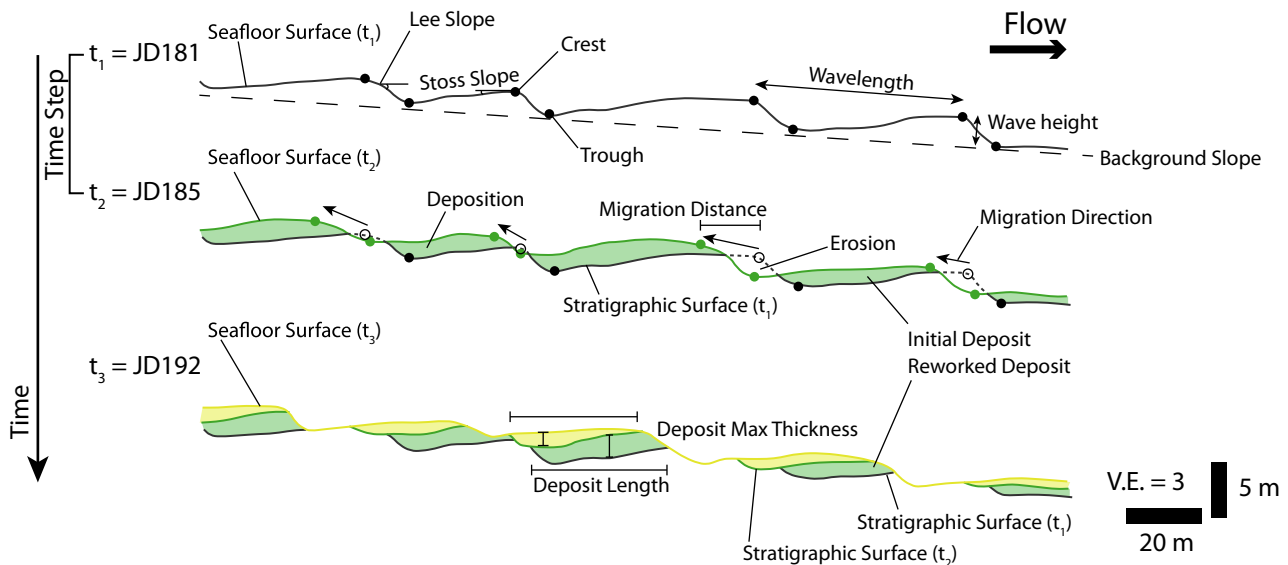
Fig. 6. The methodology for generating stratigraphic reconstructions and analyzing repeat-bathymetric datasets using an example from a segment along the Squamish prodelta southern channel (part of profiles indicated by the blue-dashed line in Fig. 2C). Bedform morphological attributes (wavelength, wave height and slope angles) were obtained from individual surveys. Subsequent surveys were stacked in order to determine areas of erosion and deposition resulting from bedform migration, and the ultimate preservation of deposits in the stratigraphic record. The length and thickness of initial deposits associated with each time step were measured, as well as the dimensions of reworked deposits in the final reconstructed stratigraphy.

(2018). For this study the cores were X-rayed and re-examined to ensure consistent analysis with ancient deposits, which included visual inspection and logging to document grain-size distributions, bed thicknesses and sedimentary features.

Outcrop characterization

Field work was conducted at Twin Beaches Peninsula on Gabriola Island to capture the nature of the outcrop and characterize deposits within the succession. Lithology was mapped around the peninsula using a differential GPS (global positioning system) and measurements of bedding orientation and palaeoflow indicators were collected. Drone images and structure-from-motion photogrammetry software were used to create high resolution 3D outcrop models for delineating and measuring the geometries of sedimentary units (c.f. Nesbit *et al.*, 2018). The architecture of deposits was further established through scaled field sketches and photomosaics. Detailed measured section, field observations and photographs were used to document the sedimentological characteristics of deposits.

RESULTS: MODERN

Bedform morphology, migration history and stratigraphic evolution

Observations: Squamish prodelta
Bedforms are crescentic on the Squamish prodelta and develop a sinuous planform as flows lose confinement on the terminal lobe (Fig. 2A). Morphological measurements from individual surveys indicate that bedforms are characterized by 14 to 122 m wavelengths (average 55 m), 0.3 to 4.3 m wave heights (average 1.6 m), and are either contained within *ca* 80 m wide channels or extend for 200 to 300 m across lobes (Figs 2A, 2D, 7A and 7B). Cross-sectional profiles through bedforms are downslope asymmetric with steeper lee compared to stoss slopes, reaching angles between 2.3° to 29° (average 13.8°) and 0° to 4.2° (average 0.9°), respectively (Figs 2D and 7B).

The upslope movement of bedform crests is clearly evident and can be traced between repeat surveys (Figs 2C, 2D and 6; see Appendix S2 for comparison of bedform positions and profiles between surveys). Because no delta lip failures occurred in the southern channel during this
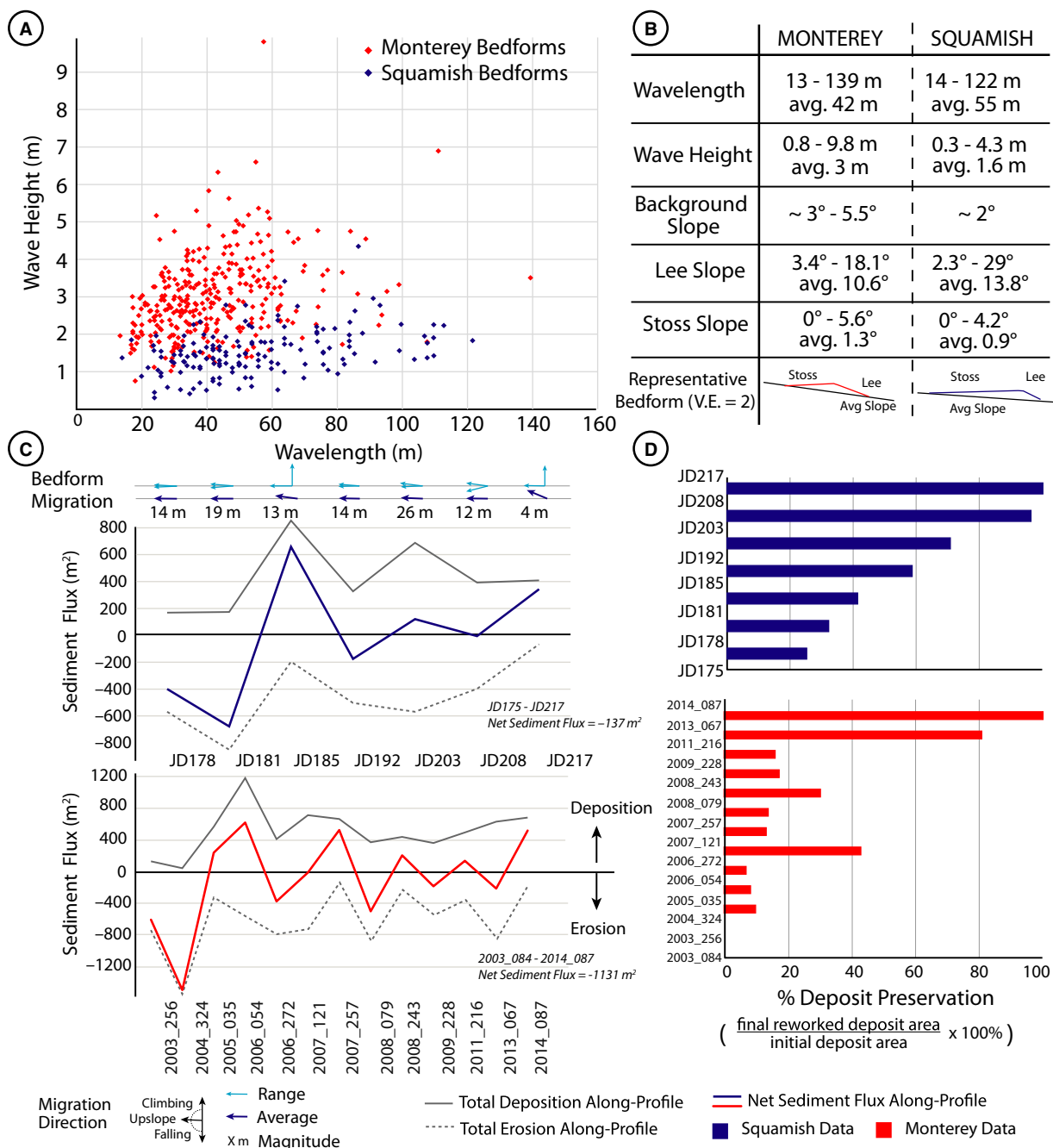
Fig. 7. (A) Wavelength versus wave height of bedforms measured from dip-oriented profiles along axial channels from the Squamish prodelta and Upper Monterey Canyon datasets. See Appendix S5 for tabulated dimensions. (B) Comparison of bedform morphology from the Upper Monterey Canyon and Squamish prodelta. Morphological attributes are tabulated for the bedforms in (A). *Slope values are listed as magnitudes. Lee slope dip directions are consistent with the background slope while stoss slopes generally dip in the opposite direction, but in some cases have low-angle inclination in the same direction as the background slope. (C) Total erosion, total deposition and net sediment flux between each survey time step along dip-oriented profiles from the two datasets. Average crest migration distance and arrows representing crest migration direction are also shown where it could be determined between Squamish prodelta surveys. (D) Deposit preservation expressed by the reworked deposit area in the final stratigraphy as a percent of the initial deposit area for each time step. These graphs indicate a significant amount of deposit reworking, which results in low preservation of older stratigraphy.

time, flow events that interact with bedforms are interpreted as turbidity currents (Clare *et al.*, 2016). Variable proportions of lee-side erosion and stoss-side deposition on bedforms produced upslope migration between daily surveys over distances of metres to tens of metres with slight angles of climb or fall (average 0.2° to 29° of climb across profiles, between 14° of fall and 90° of climb for individual bedforms; Fig. 7C). Along a dip-oriented profile of the channel thalweg, a combination of erosion and deposition occurs between all survey time steps; however, the system fluctuates between net erosional or net depositional conditions. Erosion on the lee-side of bedforms led to reworking of previous stratigraphy where up to 75% of deposits (average 39%) associated with a particular time step are removed over the entire surveyed time interval (Fig. 7D).

Observations: Upper Monterey Canyon
In the Upper Monterey Canyon, a *ca* 400 m wide, steep (4.5° to 5.5°) area covered by sinuous bedforms leads into a narrower (*ca* 140 m), lower gradient (3.0° to 3.5°) channel containing crescentic bedforms (Fig. 3B). Bedforms have 13 to 139 m (average 42 m) wavelengths, 0.8 to 9.8 m (average 3 m) wave heights, 3.4° to 18.1° (average 10.6°) lee slopes, 0 to 5.6° (average 1.3°) stoss slopes, and are predominantly downslope asymmetric (Figs 3E, 7A and 7B).

The temporal resolution of surveys is often not sufficient to resolve bedform migration in the Monterey Canyon. Bedforms are completely reworked between surveys making it difficult to correlate individual crests, although in some instances upslope movement is evident (Fig. 3C and E; see Appendix S3 for comparison of bedform positions and profiles between surveys). Upslope migration, facilitated by erosion on the lee-side and deposition on the stoss-side of bedforms, is better documented over a shorter, 32 day time period in a study of the Upper Monterey Canyon by Smith *et al.* (2007). Seafloor changes are likely a result of sediment gravity flows or mass movement events, which have been previously attributed to coarse-grained sediment transport in the proximal canyon and directly observed further downslope (Smith *et al.*, 2007; Paull *et al.*, 2010; Paull *et al.*, 2018). It is unclear whether all of the observed deposition occurs in association with bedforms; however, subsequent reworking by bedforms appears to dominate local patterns of erosion/deposition and the stratigraphic evolution between surveys regardless of the initial mode of deposition (Fig. 3C). Cumulative sediment flux along the channel thalweg varies from net erosional to net depositional conditions between survey time steps (Fig. 7C). Significant erosion causes complete removal or poor preservation (average 26%) of stratigraphy associated with a specific time period (Fig. 7D).

Integration and interpretations
Bedforms of similar scale and morphology (planform and cross-sectional) are present in the Squamish prodelta and Upper Monterey Canyon, and are additionally consistent with numerical modelling and other seafloor observations of sandy cyclic steps (e.g. Cartigny *et al.*, 2011; Kostic, 2011; Normandeau *et al.*, 2016; Symons *et al.*, 2016; Covault *et al.*, 2017; Slootman & Cartigny, 2020). The bedforms observed in the Upper Monterey Canyon are more symmetrical and have smaller aspect ratios (length/height) compared to those measured on the Squamish prodelta (Fig. 7A and B). These morphological differences could reflect the steeper slope gradient and/or specific properties of flows (for example, discharge, grain size, Froude number and gradient Richardson number) in the proximal reaches of the Monterey Canyon (Cartigny *et al.*, 2011; Fricke *et al.*, 2015; Normandeau *et al.*, 2016; Slootman & Cartigny, 2020). A combination of lee-side erosion and stoss-side deposition ensures high levels of deposit reworking, sediment transport and low-aggradation in both settings (cf. Hage *et al.*, 2018; Vendettuoli *et al.*, 2019). Although significant erosion, and in some cases net erosion, is observed over both surveyed areas, variations in sediment flux across bedforms and through time result in deposition but poor preservation of stratigraphy (Figs 7C, 7D, 9A and 10A).

Deposit geometry and architecture

Observations: Squamish prodelta
Bedform deposits reconstructed by stacking repeat bathymetric surveys from the Squamish prodelta consist of discontinuous sedimentary bodies that are 4 to 289 m long downslope (median: 22 m), 2 to 191 m wide across slope (median: 28 m) and up to 2.3 m thick (median: 0.6 m; Figs 8 and 9). Initial deposits are generally similar in downslope length to the stoss side of bedforms (representing *ca* 60% of the bedform's wavelength) with thicknesses approximately half that of bedform heights (Fig. 8D).

However, comparison of deposit geometry between surveys indicates that deposit length and thickness decrease over time, with median values decreasing by 13 to 26% and 0 to 8%, respectively (Fig. 8B to D; see Appendix S4 for videos showing the stratigraphic evolution along profiles). Strike-oriented cross-sections contain slightly longer and thinner deposits than dip and oblique-oriented sections (Fig. 9).

Individual sedimentary bodies in final stratigraphic reconstructions are trough-shaped with crescentic or oval planform geometries, and lenticular, sigmoidal/wedge-shaped or tabular in cross-section (Fig. 9). Erosional bounding surfaces at the base of deposits dip in all directions but are most commonly oriented upslope at angles <10°. In dip and oblique-oriented sections, bedform deposits are more asymmetrical lenticular and sigmoidal with steeper upslope basal surfaces (dipping up to 30°) that erosionally truncate underlying strata. Subsequent units are offset upslope forming low-angle backset stacking patterns. Variably nested symmetrical lenticular, wedge-shaped and occasional tabular bedform deposits are more commonly observed in strike-oriented sections.

Observations: Upper Monterey Canyon

Stratigraphic reconstructions from the Upper Monterey Canyon are comprised of nested bedform deposits with downslope lengths between 6 m and 260 m (median: 18 m), across slope widths between 3 m and 90 m (median: 15) and maximum thickness up to 3.1 m (median: 0.5 m; Figs 8 and 10; see Appendix S4 for videos showing the stratigraphic evolution along profiles). In general, initial deposits are similar in downslope length to the stoss side of bedforms (representing *ca* 60% of the bedform's wavelength) with thicknesses approximately a third of bedform heights (Fig. 8D). Deposit dimensions in the final stratigraphy are typically smaller than measurements of initially deposited units (reduction in median length by 13 to 28% and median thickness by 4 to 45%) and exhibit comparable sizes regardless of perspective.

Deposit architecture is quite irregular, but can be broadly described as lenticular in cross-section (Fig. 10). Basal bounding surfaces are often erosional and dip in all directions, however, they are steepest at the upslope head and edges of deposits. Reconstructions from dip and obliquely-oriented profiles contain slightly asymmetrical lenticular to sigmoidal deposits with locally apparent backstep and forestep stacking.

Strike-oriented profiles contain vertically stacked and laterally offset symmetrical lenticular deposits as well as wedge-shaped deposits at channel or scour margins.

Integration and interpretations

Sedimentary bodies of comparable size and architecture are observed in reconstructed stratigraphy from bedforms in the Squamish prodelta and Upper Monterey Canyon, despite encompassing different time periods (days versus years) and potentially different numbers of flows (Fig. 5A). Reconstructed units reflect deposition in the trough and on the stoss side of bedforms and can preserve part of the bedforms' stoss and, in some cases, lee slopes (Figs 6 and 8D). Minor differences between datasets are related to the morphology of formative bedforms and their stratigraphic evolution. For example, units initially deposited in the Upper Monterey Canyon are slightly shorter, thicker and have broader distributions than those deposited in the Squamish prodelta (Fig. 8). This could reflect the shorter wavelength and greater height of Upper Monterey Canyon bedforms, as well as the likely more reworked and composite nature of deposits due to more significant erosion and longer time durations between surveys (Fig. 7). However, reworking of initial strata in both settings results in smaller remnant units being preserved in the final reconstructions with comparable dimensions (Fig. 8). Deposit geometry and stacking in dip-oriented, oblique-oriented and strike-oriented sections, although similar to the Squamish prodelta, is more irregular in the Upper Monterey Canyon possibly due to greater deposit amalgamation and/or more erosive and fluctuating flow conditions in the Monterey system. Within datasets, differences in the architecture and, to a minor extent, dimensions of deposits in 2D cross-sections are related to the cross-section orientation through stratigraphy (Figs 8 to 10).

Deposit sedimentological characteristics

Observations: Squamish prodelta

Sediment cores through bedform deposits on the Squamish prodelta are primarily composed of thick-bedded amalgamated sand (L1), with silty sand (L2.5) typically preserved at the bottom of cores or occasionally interbedded with thicker sand beds of L1 (Table 1; Fig. 11A and B). Coarse-grained sand beds are 10 to 100 cm thick, slightly normally graded, amalgamated, and largely structureless with some subtle
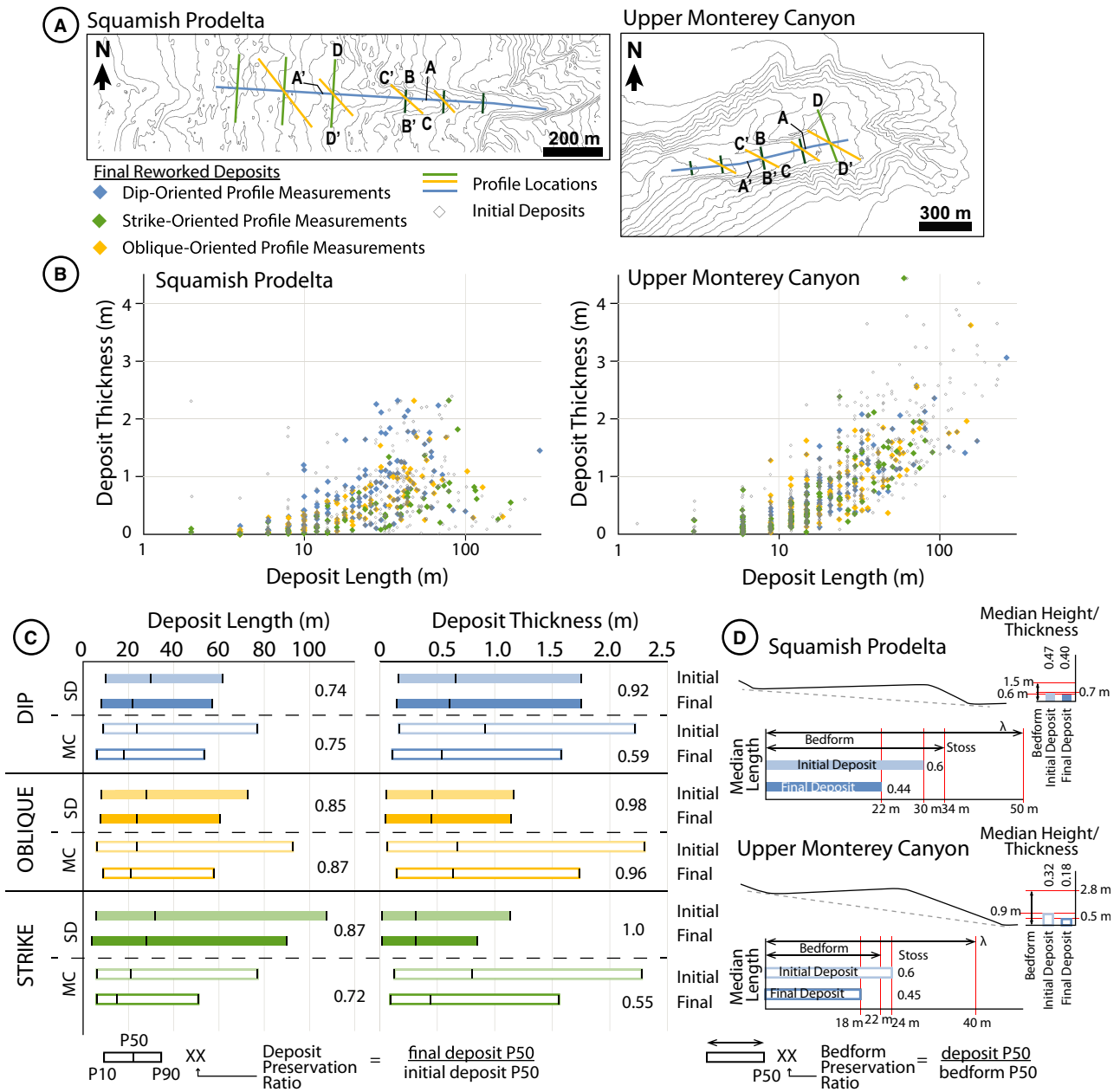
Fig. 8. (A) Location of stratigraphic reconstruction profiles in the Squamish prodelta and Upper Monterey Canyon coloured by orientation. Examples shown in Figs 9 and 10 are labelled. (B) Length and thickness measurements compiled from deposits in final stratigraphic reconstructions for the profile locations in (A). The dimension distributions of associated initial deposits are also shown. Note the logarithmic scale on the x-axes. (C) Comparison of deposit geometries and evolution in dip, oblique and strike-oriented sections between the Squamish prodelta (SD) and the Upper Monterey Canyon (MC). The ratio of final and initial deposit geometry P50 values provides a general metric for deposit preservation. (D) Rough comparison of bedform dimensions (wavelength, stoss slope length and wave height) to the length and thickness of initial and reworked, final deposits. The ratio of final and initial deposit geometry P50 values to bedform wavelength and wave height P50 values provides a general metric for bedform preservation. See Appendix S5 for deposit dimension datasets.

internal laminations and grain-size breaks observed in cores and X-ray images. Equivalent facies are found in all sediment cores; however, individual beds cannot be correlated between cores despite their close spacing (cf. Hage *et al.*, 2018). Similar characteristics have been reported
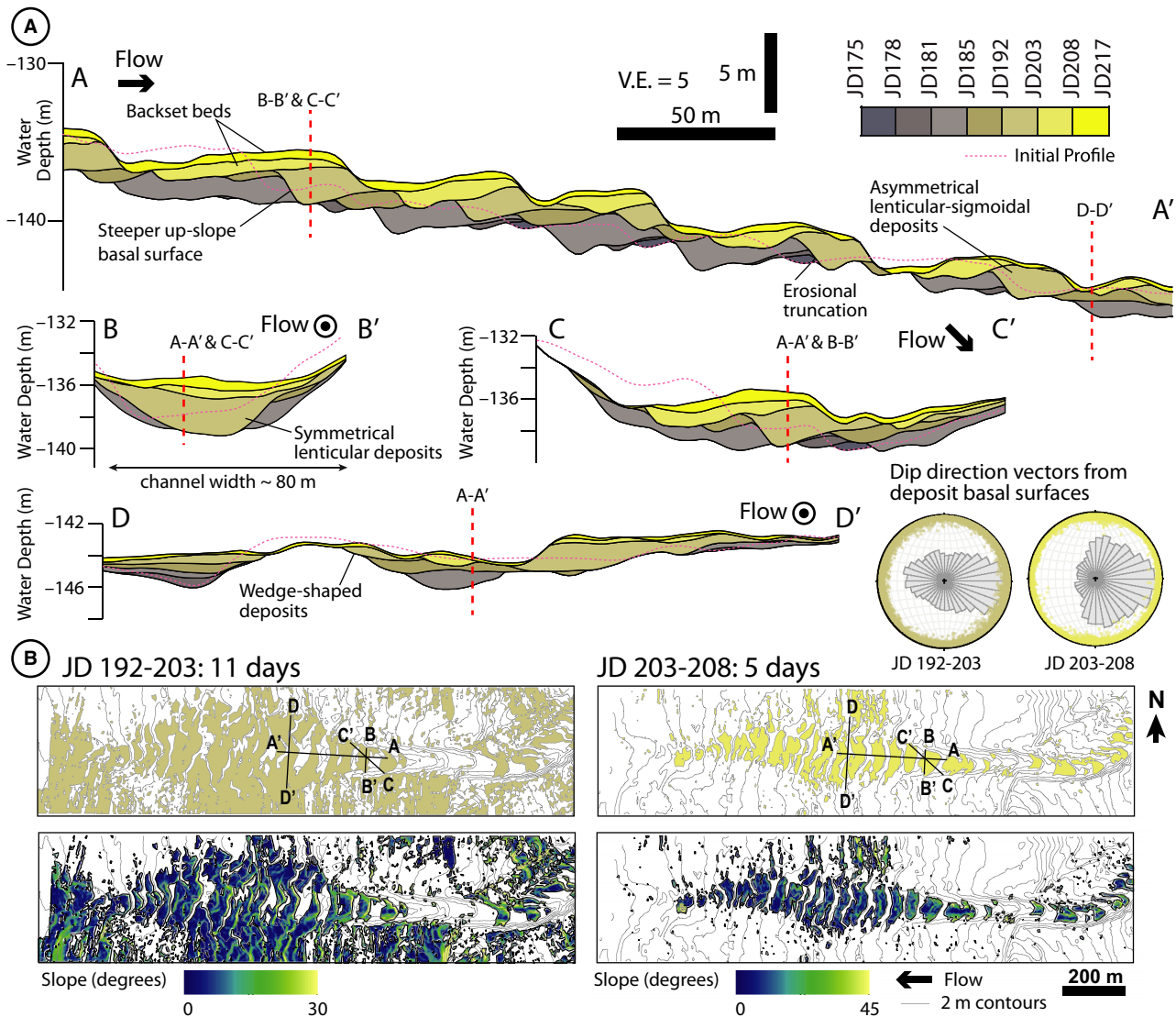
Fig. 9. Reconstructed bedform deposit architecture and geometries from the Squamish prodelta. (A) Examples of stratigraphic reconstructions from dip (A–A'), oblique (C–C') and strike-oriented (B–B' and D–D') perspectives. The initial profile (JD175) is overlain on each (pink-dashed line) and indicates overall low-aggradation. Colours correspond to the time step in which units were deposited. Section locations are shown on maps in (B). See Appendix S4 for videos of stratigraphic reconstruction generation. (B) Planform distribution maps of remnant deposits associated with a specific time step (top) and corresponding slope maps (bottom) for deposit basal surfaces. Stereonets and rose diagrams for deposit basal surfaces show that surfaces dominantly dip shallowly upslope relative to the background slope but may dip in all directions.

in cores obtained from Squamish prodelta lobes (Stacey *et al.*, 2019).

Observations: Upper Monterey Canyon
Sediment cores from the Monterey Canyon within and downslope of the study area have been previously described, although not examined in this study (Paull *et al.*, 2005; Paull *et al.*, 2010). Cores from the axial Monterey

channel are quite variable, containing 40 to 200 cm thick massive, normally graded sand beds that are more poorly sorted at their bases and often contain floating gravel and mud clasts.

Integration and interpretations
Sediment cores from the Squamish prodelta and Upper Monterey Canyon reveal that the examined bedforms are dominantly composed of coarse-
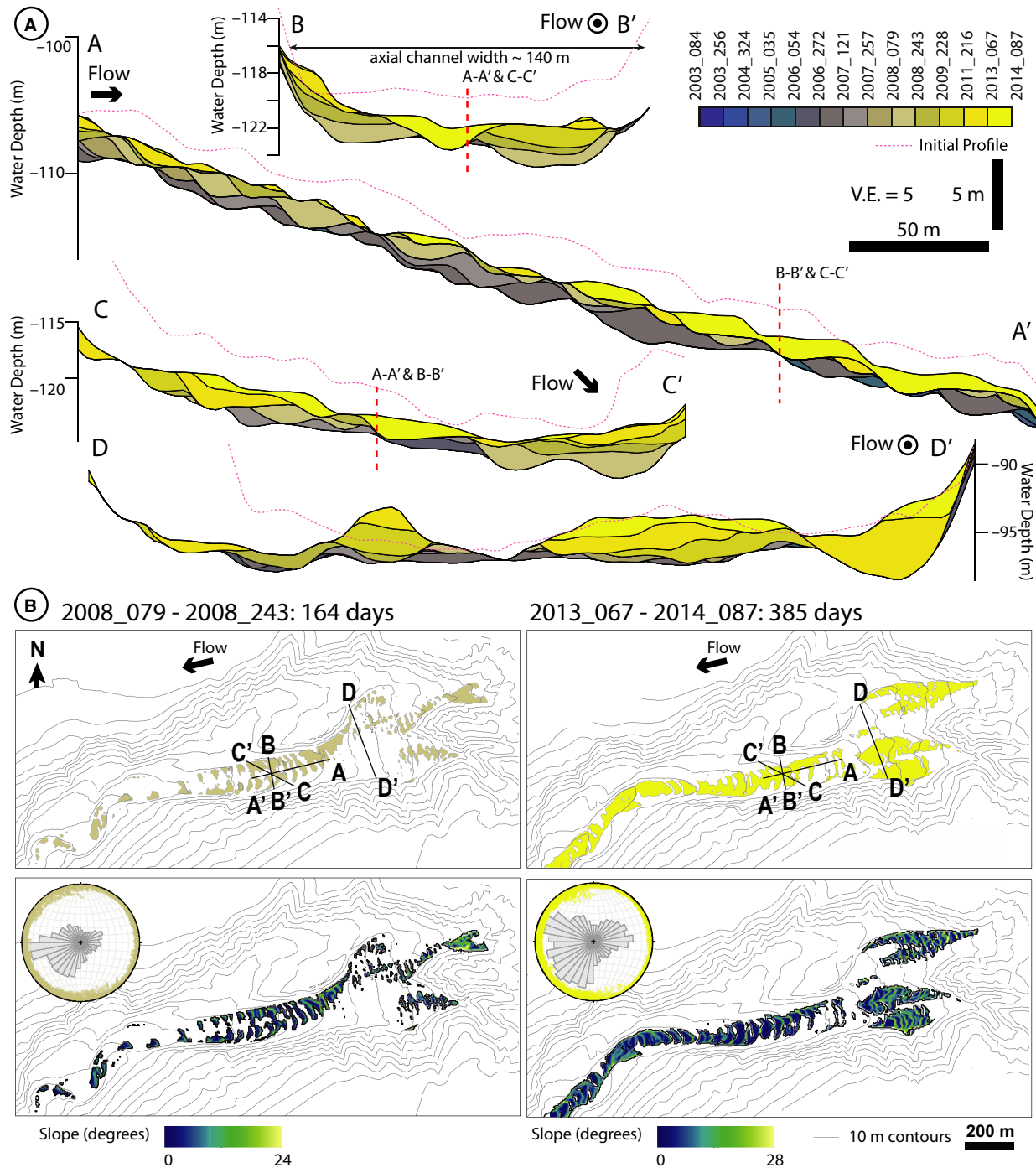
Fig. 10. Reconstructed bedform deposit architecture and geometries from the Upper Monterey Canyon. (A) Examples of stratigraphic reconstructions from dip (A–A'), oblique (C–C') and strike-oriented (B–B' and D–D') perspectives. Colours correspond to the time step in which units were deposited. The initial profile (2003_084) is overlain on each (pink-dashed line) and reveals overall net-erosion over the surveyed time period. Likewise, the absence of blue colours in stratigraphic reconstructions indicates poor preservation of initial stratigraphy. Section locations are shown on maps in (B). See Appendix S4 for videos of stratigraphic reconstruction generation. (B) Planform distribution maps of remnant deposits associated with a specific time step (top) and corresponding slope maps for deposit basal surfaces (bottom). Stereonets and rose diagrams for deposit basal surfaces show that surfaces dip largely up-slope or down-slope relative to the background slope, indicating preservation of both lee and stoss sides of bedforms.

Table 1. Lithofacies descriptions.

| | Description | | |
Lithofacies	Nanaimo Group outcrop	Squamish sediment cores	Interpretation
L1: Medium – thick bedded amalgamated sand/sandstone	*Lithology*: Fine – coarse (average medium) sandstone. Beds are normally graded, often only the coarsest grain-size fraction from maximum grain sizes of very coarse sand – granules at bed bases to medium – coarse sand (rarely fine) at bed tops *Thickness*: 20–200 cm thick beds in up to 25 m thick packages *Sedimentary features*: Massive sandstone with some localized, crude stratification (internal amalgamation surfaces, foresets, backsets, spaced stratification). Floating granules sometimes present in lower portion of beds. Mudstone clasts also common at the base or floating in lenses within beds. Sharp undulatory bed contacts, in some cases loaded	L2.5: Silty Sand *Lithology*: Medium – coarse sand. Most beds are slightly coarse-tail normally graded with maximum grain sizes of very coarse sand – pebbles at bed bases to coarse sand (rarely medium) at bed tops. Inverse grading at the bottom of a few beds *Thickness*: 5–100 cm thick beds in up to 260 cm successions within 128–329 cm long cores *Sedimentary features*: Massive sands with rare internal laminations. Common floating extrabasinal pebbles (up to 3.5 cm) and granules, particularly at the lower portions of beds. Occasional mud rip-up clasts and woody debris. Sharp bed contacts	High-density turbidity currents, traction deposition with potentially high near-bed sediment concentrations (Lowe, 1982; Talling *et al.*, 2012)
L2: Thin – medium bedded sandstone and siltstone	*Lithology*: Fine – coarse sandstone and siltstone. Some beds normally grade from medium or coarse sandstone to very fine sandstone or siltstone *Thickness*: 1–15 cm thick sandstone beds interbedded with siltstone in packages from 20 cm to 5 m thick *Sedimentary features*: Sandstone beds are typically massive or planar laminated, often with rippled bed tops. A few beds are cross-stratified. Bedding is planar or lenticular with sharp or loaded contacts	L2.5: Silty Sand *Lithology*: Silty fine sand *Thickness*: 5–75 cm sand beds in up to 140 cm successions *Sedimentary features*: Some planar, ripple and wavy laminations present, as well as rare wood fragments. Sharp bed contacts	Traction and suspension deposition from high-density turbidity currents (some bypassing) and/or low-density turbidity currents (Bouma, 1962; Mutti & Normark, 1987; Stevenson *et al.*, 2015). L2.5 may also include deposition from debris or hybrid flows (Haughton *et al.*, 2009; Talling *et al.*, 2012)
L3: Siltstone with limited sandstone	*Lithology*: Siltstone with limited very fine – fine sandstone *Thickness*: Sandstone beds are up to a few centimetres thick in siltstone dominated packages up to 5 m thick *Sedimentary features*: Some beds are planar laminated and/or rippled	L2.5 Silty Sand *Lithology*: Silty fine sand *Thickness*: 5–75 cm sand beds in up to 140 cm successions *Sedimentary features*: Some planar, ripple and wavy laminations present, as well as rare wood fragments. Sharp bed contacts	Suspension deposition from low-density turbidity currents and hemipelagic settling (Talling *et al.*, 2012)

Table 1. (continued)

Lithofacies	Description		Interpretation
	Nanaimo Group outcrop	Squamish sediment cores	
L4: Mudstone clast conglomerate	*Lithology*: Poorly sorted coarse sandstone matrix with <20 cm mudstone clasts	No equivalent facies observed	Debris flow deposition (Talling *et al.*, 2012)
	Thickness: 70 cm to 5 m thick beds		
	Sedimentary features: Structureless, disorganized fabric and sharp bed contacts		
L5: Chaotically bedded mudstone with sandstone beds	*Lithology*: Mudstone, siltstone and sandstone blocks/beds	No equivalent facies observed	Mass wasting (Tripsanas *et al.*, 2008)
	Thickness: 0.5–5.0 m thick intervals		
	Sedimentary features: Contorted mudstone fabric and sandstone beds. Intrabasinal sandstone and thinly bedded sandstone and siltstone blocks as well as rare floating extrabasinal granules and pebbles		

grained sandy units (L1) with comparable thicknesses to sedimentary bodies generated in stratigraphic reconstructions (Fig. 8). These units resemble the deposits of high-density turbidity currents (c.f. Lowe, 1982) with high near-bed sediment concentrations, which suppress turbulence and lead to the formation of structureless deposits (Sumner *et al.*, 2008; Talling *et al.*, 2012; Hage *et al.*, 2018; Paull *et al.*, 2018). The origin of silty sands (L2.5) observed only in the Squamish prodelta cores is uncertain and interpreted to result from sediment gravity flow processes (Talling *et al.*, 2012) and/or river plume suspension settling (Stacey *et al.*, 2019), possibly during periods of lower sediment delivery to the prodelta (such as in winter months) or when flows are bypassing or constricted to one side of the channel.

RESULTS: ANCIENT

Twin Beaches Peninsula stratigraphy

Observations
The Gabriola Formation at Twin Beaches Peninsula is exposed in NNW–NNE shallowly dipping (*ca* 7° to 12°) strata in quasi-horizontal beach and vertical wall outcrops around the peninsula that provide variably-oriented exposures (Fig. 12E). The peninsula is made up of a *ca* 65 m thick, at least 1.2 km wide succession of dominantly thick-bedded, medium–coarse grained sandstones (L1), in some areas interbedded with more heterolithic (L2) and mudstone-clast-rich deposits (L4; Figs 11C, 12 and 13; Table 1). At the base of the succession, these units sharply overlie and are lateral to siltstone-dominated deposits (L3) and chaotically bedded mudstone with sandstone beds (L5), giving the peninsula an overall channelform shape (Fig. 12; Table 1). However, internal architecture and lateral facies relationships are difficult to differentiate due to limited exposures (20 to 120 m wide) in the intertidal zone and the abundance of amalgamated sandstone. Small-scale stratification, including backsets and ripple-dune scale foresets, indicate south-west to north (187° to 12°) palaeoflow directions (average *ca* 290° WNW) at Twin Beaches Peninsula, which are generally consistent with measurements of the Gabriola Formation at other locations on Gabriola Island (Figs 4B and 12E).
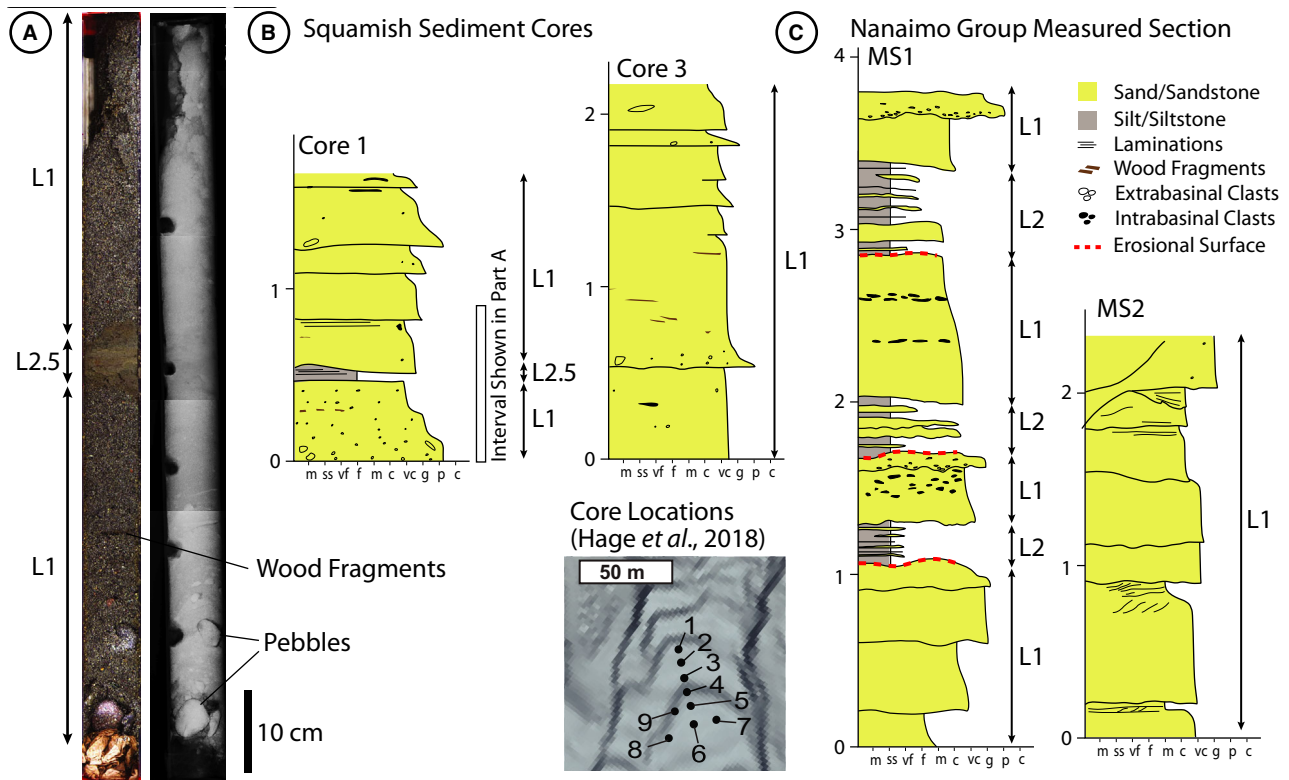
Fig. 11. (A) and (B) Sediment cores obtained from upslope-migrating bedforms within the central channel on the Squamish Delta. (A) Photograph and X-radiograph of a segment of the sediment core shown in (B). (B) Examples of sediment core logs. Similar facies are described by Hage *et al.* (2018). (C) Measured section from Nanaimo Group deposits exposed on the Twin Beaches Peninsula. See locations in Fig. 12E.

Interpretations

Large-scale channel-form architecture dominated by amalgamated coarse-grained turbidites (L1) is consistent with deposition in a deep-water slope conduit (cf. Gardner *et al.*, 2003; Hodgson *et al.*, 2011; Macauley & Hubbard, 2013), as well as previous interpretations of the Gabriola Formation and older coarse-grained formations on Gabriola Island (England & Hiscott, 1992; Englert *et al.*, 2018). Underlying siltstone-dominated (L3) and discordant/disturbed (L5) strata are interpreted as low-energy slope deposits resulting largely from suspension settling (Talling *et al.*, 2012) and slump deposits related to mass-wasting processes (Tripsanas *et al.*, 2008), respectively. A refined regional context, which was not the focus here, would be needed to define a more precise depositional environment or slope position for the succession exposed at Twin Beaches Peninsula. However, the Gabriola Formation extends along the outcrop trend for *ca* 70 km to the southeast up palaeo-depositional dip, suggesting a minimum distance from the shoreline for the studied deposits at water depths of hundreds of metres (England & Hiscott, 1992).

Deposit geometry and architecture

Observations

A considerable portion of the succession contains relatively small-scale discontinuous sedimentary bodies (Fig. 13). These sedimentary bodies are 2 to 84 m (median: 9.5 m) long and 0.1 to 4.8 m (median: 0.64 m) thick (Fig. 14A). In some areas highly amalgamated sandstones form larger packages that can be >100 m long, several metres to tens of metres thick, and contain variably mappable internal surfaces; however, definitive units cannot be resolved due to a lack of grain-size variability along portions of key sedimentary body boundaries. There is no clear trend in deposit dimensions around the peninsula despite differences in outcrop orientation (Fig. 14B).
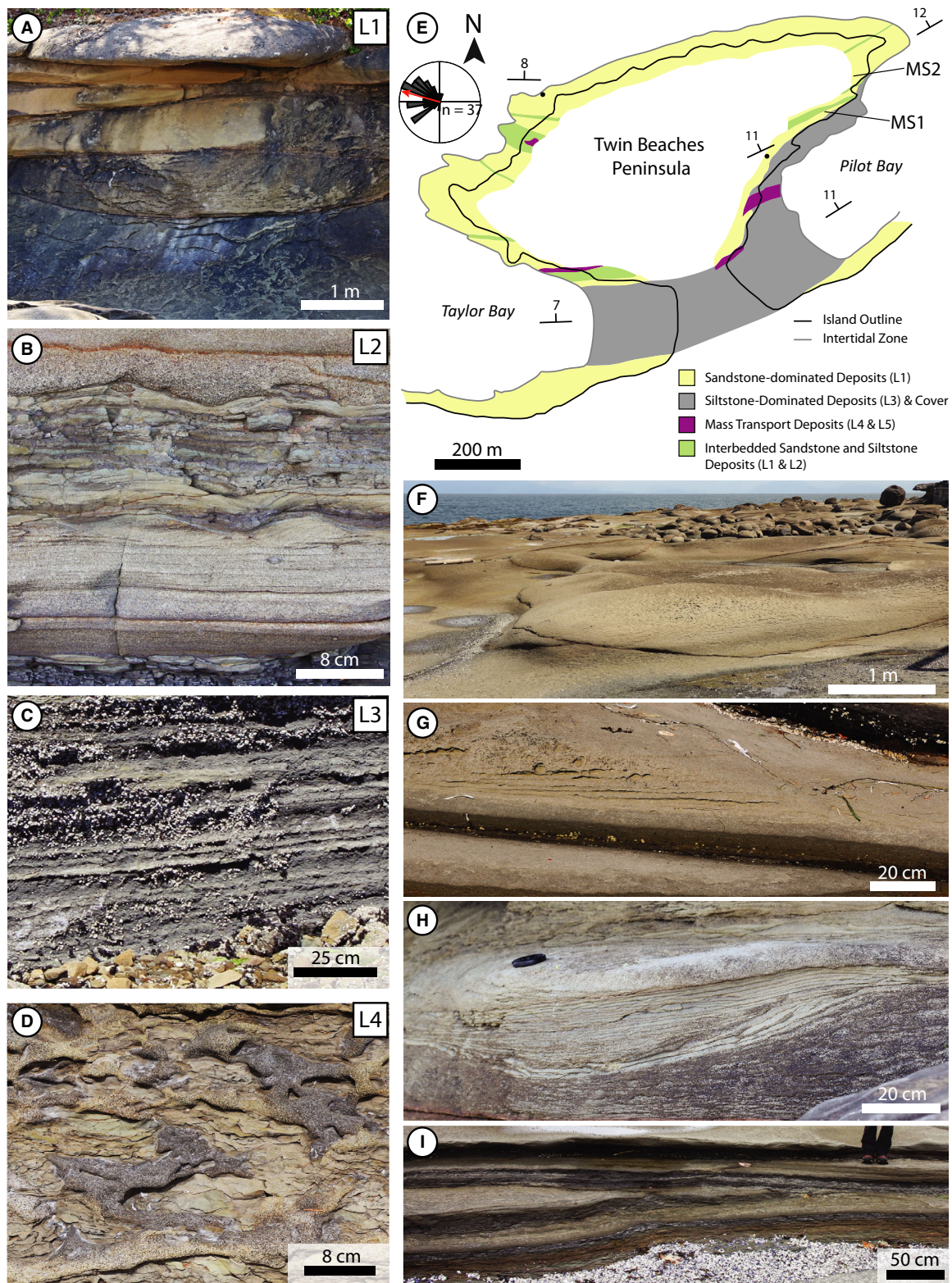
Fig. 12. (A) Lithofacies 1 – Medium–thick bedded, amalgamated sandstone. (B) Lithofacies 2 – Thin-medium bedded sandstone and siltstone. (C) Lithofacies 3 – Siltstone with thin, fine-grained sandstone beds. (D) Lithofacies 4 – Mudstone conglomerate. (E) Lithological map of strata exposed around Twin Beaches Peninsula. (F) Amalgamated sandstone (L1) exposed along the beach at the top of the peninsula. (G) and (H) Faint low-angle foresets and grain-size stratification within sandstone beds. (I) Lenticular sandstone bed within a heterolithic unit (L2).
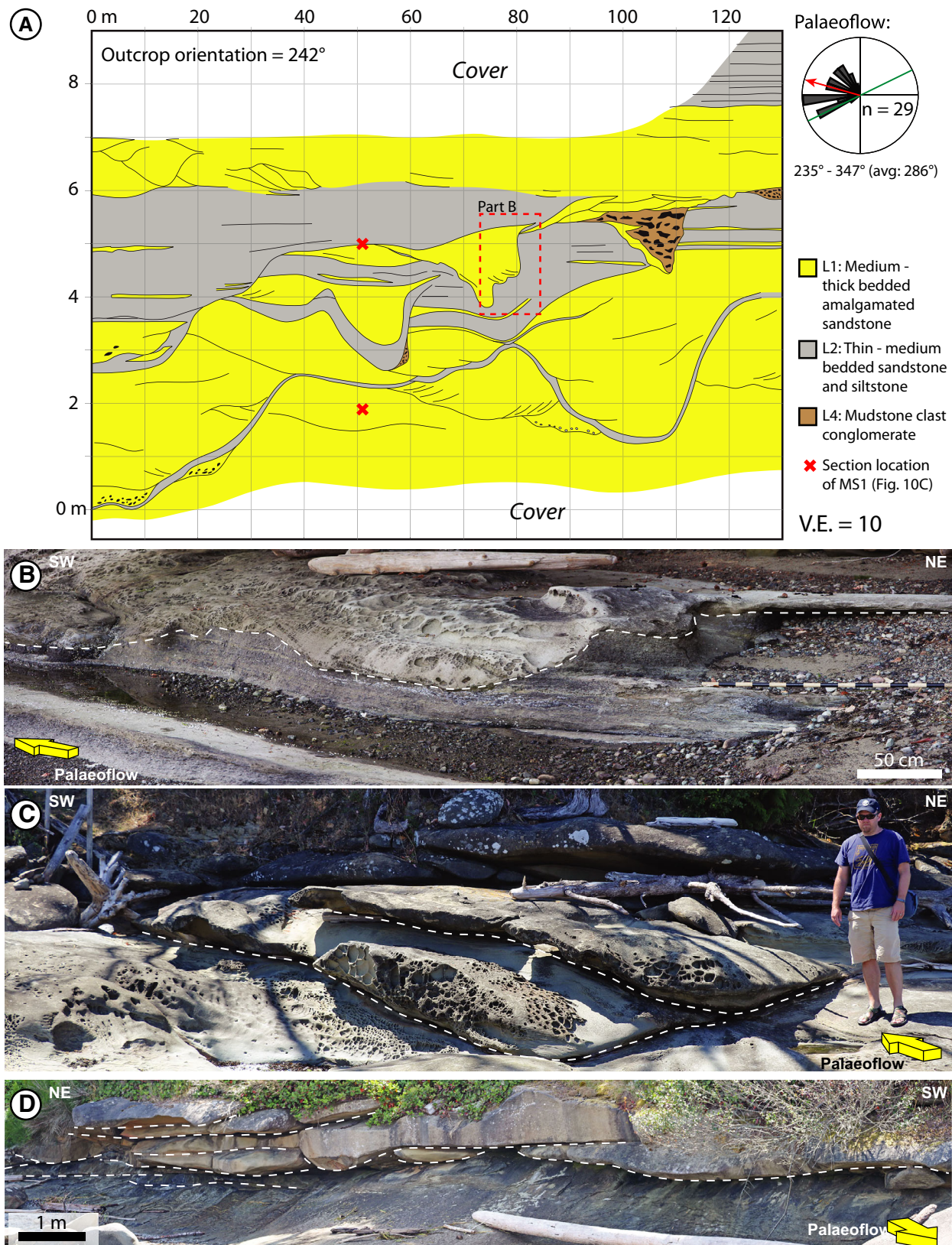
Fig. 13. (A) Scaled dip-oriented outcrop sketch of stratigraphy on the south-east corner of Twin Beaches Peninsula. (B) Steep head of a flute-shaped deposit. (C) Nested lens/wedge-shaped units. Person for scale is *ca* 1.8 m tall. (D) Broad lenticular deposits in a wall exposure.
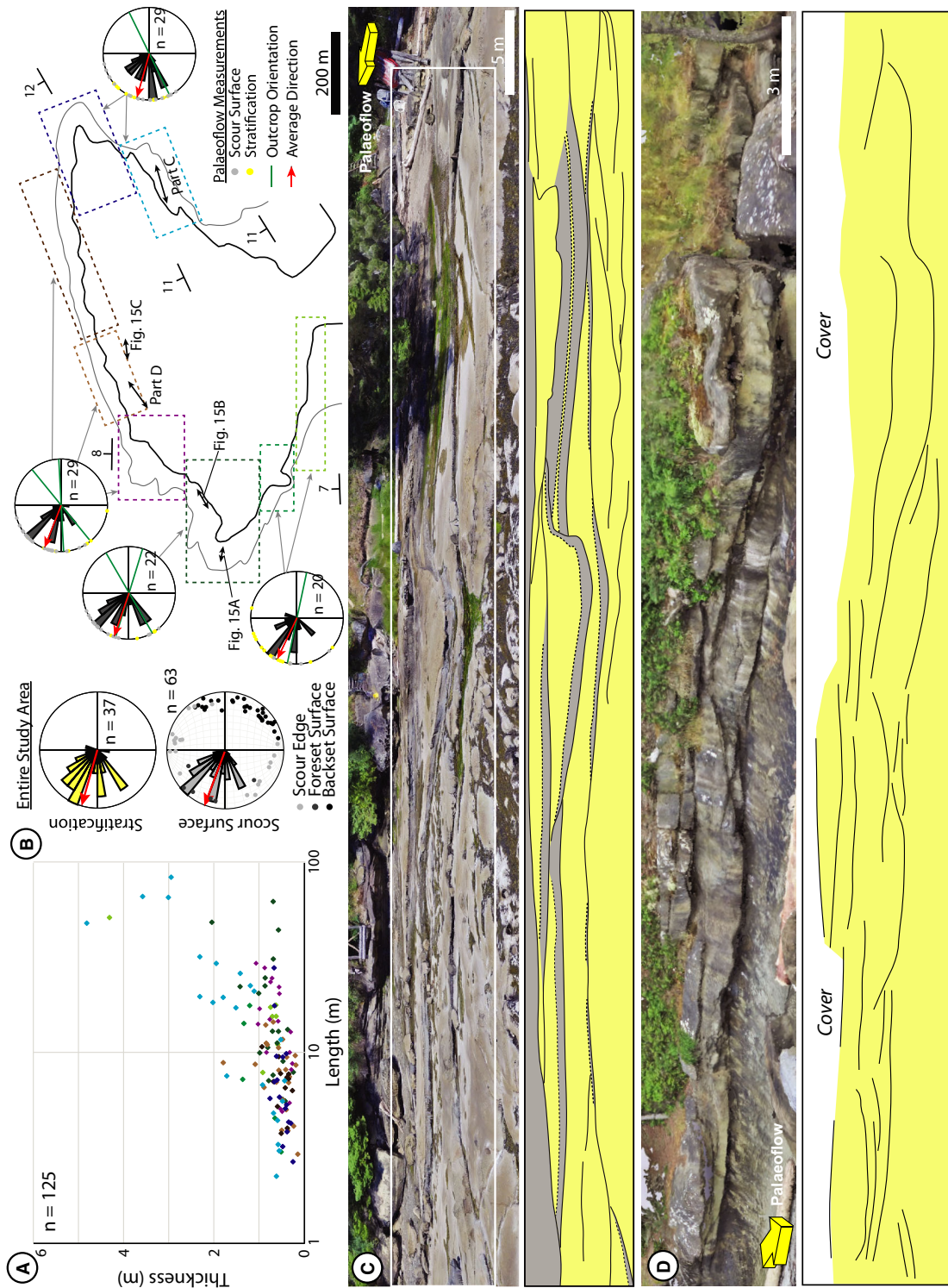
Fig. 14. (A) Geometry of deposits from around the Twin Beaches peninsula. Colours correspond to locations delineated by rectangles in (B). Note logarithmic scale on x-axis. See Appendix S5 for deposit dimensions dataset. (B) Palaeoflow measurements derived from stratification and scour surfaces around the peninsula combined and separated by location. The location and orientation of sections in (C) and (D) as well as those in Fig. 15 are also shown. (C) Oblique-dip oriented perspective and (D) strike-oriented perspective through stratigraphy shown in image captures from the drone outcrop model (top) and corresponding line drawing traces and lithology (bottom).

Fig. 15. Lenticular sedimentary bodies in (A) dip and (B) and (C) oblique oriented outcrops on the Twin Beaches Peninsula. Locations and orientations shown in Fig. 14B.

Stratigraphy is generally characterized by a variety of nested lenticular and wedge-shaped units with some more tabular geometries (Fig. 13). Deposit basal bounding surfaces are often erosional, undulatory and may include superimposed, small-scale stepped scours (Fig. 13B); basal surfaces dip in all directions, typically between 3° and 32° (average *ca* 15°) although shallowly inclined surfaces were generally difficult to measure (Fig. 14B). In some oblique and dip-oriented outcrops, flute-shaped deposits with steep upslope faces are observed to truncate underlying strata, forming a series of upslope-stepping units (Figs 13A and 14C). Other similarly oriented outcrops contain upslope-inclined lens-shaped beds that thicken upslope, (Figs 13C and 15) while strike-oriented outcrops are more dominated by lenticular and tabular deposits (Figs 13D and 14D).

Interpretations
The prevalence, size and discontinuous nature of the units suggest that they are the deposits of relatively large, three-dimensional bedforms. Nested units with erosive basal surfaces indicate subsequent reworking and are interpreted to make up successions of bedform deposit remnants. These remnant deposits are characterized by backset stacking as well as asymmetrical scour fill geometry, which are consistent with

the products attributed to supercritical flow bedforms (Alexander *et al.*, 2001; Cartigny *et al.*, 2014; Postma *et al.*, 2014; Fedele *et al.*, 2016; Slootman & Cartigny, 2020) and comparable to the cyclic step deposits reconstructed from the Squamish prodelta and upper Monterey Canyon seafloor datasets (Figs 9 and 10). Differences in architecture around the peninsula appear to relate to unit orientation relative to palaeoflow direction as well as the presence of potentially different styles of deposits (for example, degradational versus aggradational bedforms; Figs 1, 14 and 15). However, observations of architecture are also complicated by the structural dip, palaeoflow variability (commonly spanning 75° to 110°) and the nature of exposure (flat beach or vertical wall).

Bedforms interpreted as cyclic steps are observed in a variety of modern slope conduit environments (Figs 1A, 2A and 3A) including channels with variable levels of confinement (Piper *et al.*, 1985; Paull *et al.*, 2010; Maier *et al.*, 2011; Stacey *et al.*, 2019), channel-lobe transition zones (Wynn *et al.*, 2002), sandy overbanks/splays (Fildani *et al.*, 2006; Hill, 2012; Carvajal *et al.*, 2017) and intraslope lobes (Maier *et al.*, 2017). Thus, the coarse-grained succession of bedform-dominated deposits encapsulated in a composite channel-form body at Twin Beaches Peninsula can be attributed to a broad slope

conduit characterized by a bedform field or laterally migrating channels containing trains of bedforms.

Deposit sedimentological characteristics

Observations

Sedimentary bodies at Twin Beaches Peninsula are mainly composed of medium to thick beds of medium to coarse-grained, amalgamated sandstone (L1) and less commonly include mudstone-clast conglomerate (L4) and thin-medium bedded sandstone and siltstone (L2; Figs 11C, 13, 14 and 15; see Table 1 for lithofacies characteristics). The bounding surfaces of deposits are commonly erosional, and delineated by fine-grained drapes (L2) or amalgamated sandstone-on-sandstone contacts that are highlighted by beach erosion (Fig. 14C and D). Sandstone beds are normally graded, often only in the coarsest grain-size fraction, and have sharp, slightly undulatory and/or loaded contacts (Fig. 11C). Beds are largely massive with some subtle, localized sedimentary features including internal amalgamation surfaces, decimetre-scale foresets or backsets and planar stratification (Tb3a, Tb3b or Tb2, Figs 11C and 12). Mudstone clasts are common in lags at bed bases or in lenses within beds (Fig. 11C).

Interpretations

Facies are all consistent with sedimentation by partially bypassing (L2) or depositional (L1) high-density turbidity currents and occasional debris flows (L4; Talling *et al.*, 2012; Stevenson *et al.*, 2015). Interbedded drapes and scour fill (L2) are interpreted to represent deposition of lags and tails from largely bypassing flows (Fig. 11C; Stevenson *et al.*, 2015) and suggest that some sedimentary units within the succession have multi-phase histories (cf. Ito *et al.*, 2014; West *et al.*, 2019).

SYNTHESIS: MODERN AND ANCIENT RESULTS

Active channels in the Squamish prodelta and Monterey Canyon contain crescentic and sinuous, downslope asymmetric bedforms with wavelengths between 10 to 140 m and 0.3 to 9.8 m wave heights (Fig. 7). Upslope migration facilitated by variable degrees of lee-side erosion and stoss-side deposition suggest that bedforms can be classified as partially erosional to partially depositional cyclic steps (cf. Slootman &

Cartigny, 2020) and produce remnant deposits (with 0.72 to 0.87 length and 0.55 to 1.0 thickness preservation ratios) that preserve *ca* 45% of the bedform wavelength, preferentially the stoss slope (Figs 8 and 16).

Similarities are also documented between deposits in modern (Squamish prodelta and Upper Monterey Canyon stratigraphic reconstructions) and ancient (Nanaimo Group stratigraphy) datasets (Figs 5A, 16 and 17). Successions contain discontinuous, erosion-surface bound, trough-shaped sedimentary bodies on the order of tens of metres long, often <1 m (up to several metres) thick that are composed of slightly normally graded, internally structureless sands/sandstones (Figs 16 and 17; see Appendix S4 for videos of deposit stratigraphic evolution). Deposit architecture in 2D planform and vertical cross-sections through stratigraphy is variable due to deposit reworking (Fig. 17B). Dip and oblique-oriented cross-sections contain more asymmetrical lenticular and sigmoidal deposits characterized by basal bounding surfaces with overall shorter, steeper up-section (<30°) and longer, gently upslope-inclined down-section (<10°) sides (Figs 16A, 17B and 17C). Deposits are nested and offset from one another, often in an upslope direction to form backstepping stacking patterns. Strike-oriented cross-sections contain more symmetrical lenses as well as wedge-shaped and tabular deposits; basal surfaces have a range of dips from flat to <30° that are more equally oriented towards either side of the section (Fig. 17B and C). Sedimentary units may be stacked vertically, laterally offset or nested into each other. The equivalent scale, architecture and sedimentological characteristics of deposits within the Nanaimo Group succession at Twin Beaches Peninsula to those associated with bedforms in the Squamish prodelta and Upper Monterey Canyon support the hypothesis that these deposits formed by similar upslope-migrating bedforms, in this case cyclic steps (Figs 16 and 17).

Comparable findings from each study area support process-based relationships for flow–seafloor interactions and resulting stratigraphy, which pertain to multiple sedimentary environments (Fig. 5A; Symons *et al.*, 2016; Slootman & Cartigny, 2020). Seafloor datasets demonstrate the occurrence of morphologically similar cyclic step bedforms between and within different subaqueous settings spanning a range of water depths, system scales and sub-environments (lobes, channels, channel lobe transition zones, etc.; Figs 1A,
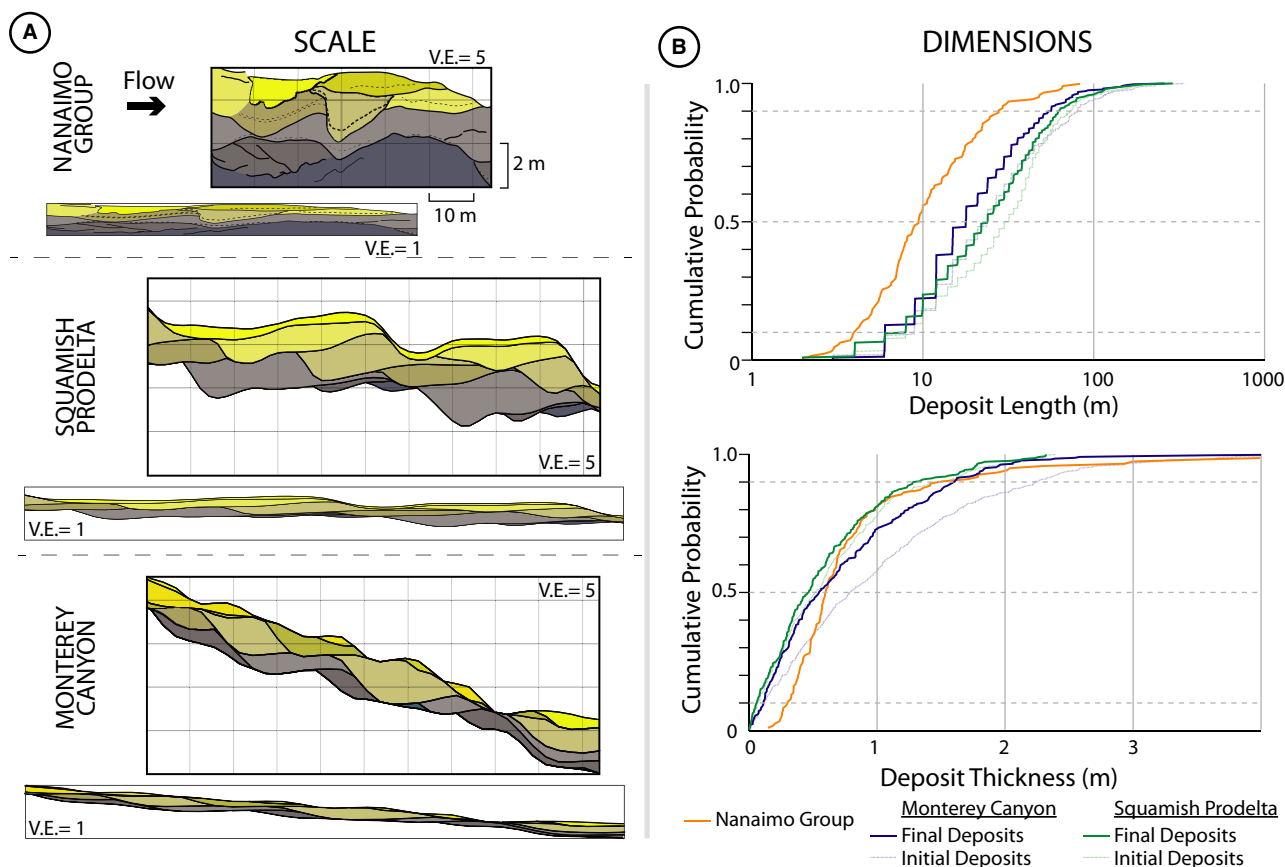
Fig. 16. Comparison of bedform deposit scale and dimensions between the investigated datasets. (A) Flow parallel outcrop sketch and stratigraphic reconstruction at the same scale with and without vertical exaggeration. (B) Cumulative probability plots of deposit length and thickness.

2A, 3A and 5A). Further, comparable bedform deposits can result despite differences in temporal scale, which may influence bed-scale characteristics due to variations in flow frequency and the increasing impact of preservation and the potential occurrence of rare flow events over longer time periods. The identification of cyclic step deposits in the ancient succession suggests that the stratigraphic products of dynamic bedforms such as those observed on modern delta fronts and canyons can be preserved over long timescales in the rock record, even under dominantly bypass conditions and where stratigraphic preservation potential is low.

DISCUSSION

Diagnostic recognition criteria

The relatively large size of seafloor bedforms and a lack of established recognition criteria for

cyclic step deposits has been used to explain their previously limited identification in ancient deep-water successions (e.g. Piper & Kontopoulos, 1994; Hage *et al.*, 2018). Based on present knowledge and the results of this study, diagnostic criteria (facies, scale and architecture) for recognition of cyclic steps in 1D, 2D and 3D exposures of coarse-grained deep-water deposits are reviewed (Figs 16 and 17).

Facies

Cyclic step deposits composed of amalgamated, massive, poorly graded sandstone (L1) and high energy interbedded sandstones and siltstones (L2) are consistent with facies traditionally ascribed to partially bypassing and waning high-density turbidity currents (Fig. 17A; Lowe, 1982; Sumner *et al.*, 2008; Talling *et al.*, 2012; Stevenson *et al.*, 2015). Similar sedimentary characteristics have been noted in the relatively few examples of cyclic step deposits interpreted from other deep-water outcrops, although in
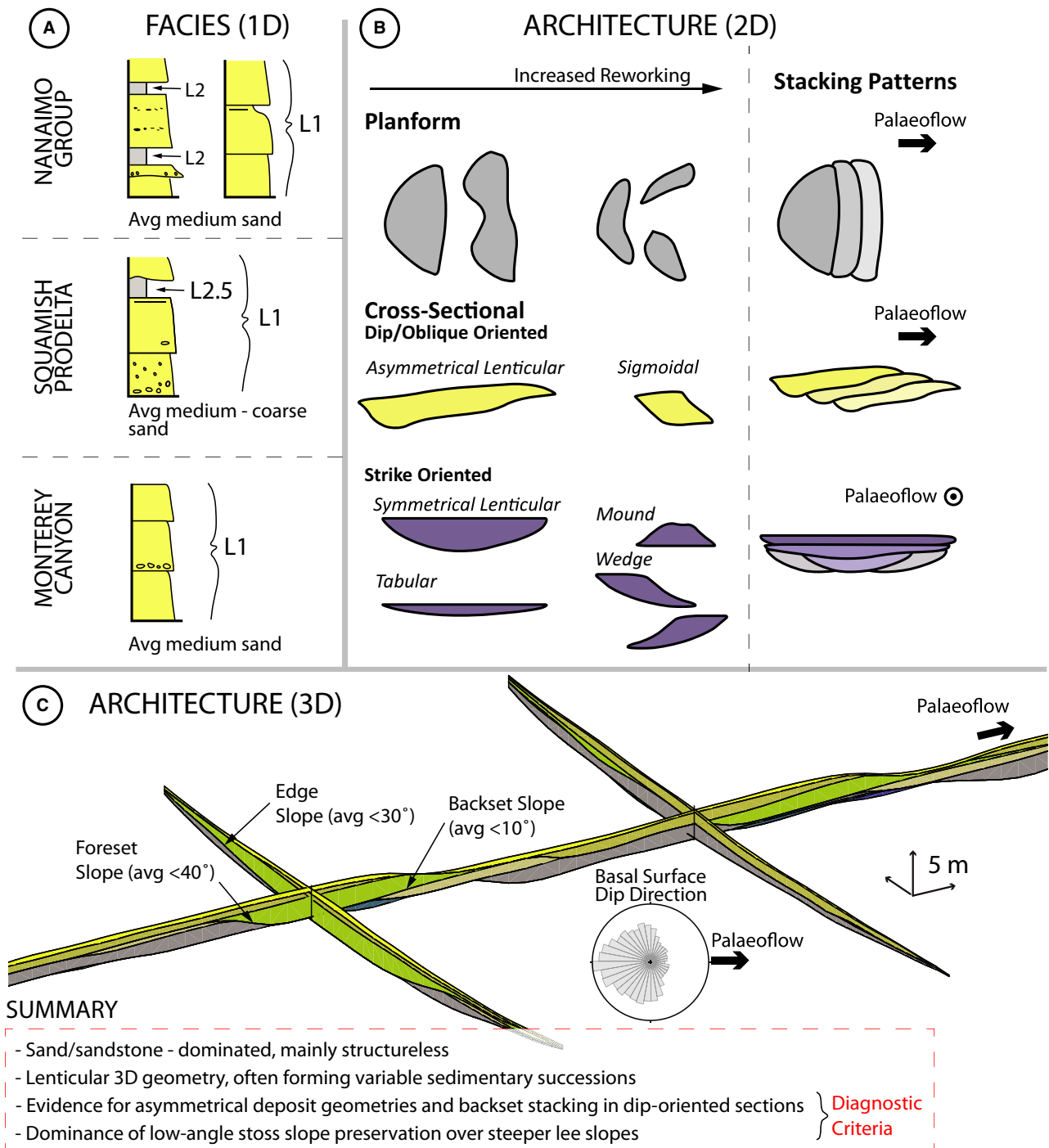
Fig. 17. Comparison of bedform deposit sedimentological and architectural characteristics between the investigated datasets. (A) Types and sequences of facies observed in vertical profiles (in core or measured section) at each location. Average grain size is indicated, although all successions contain up to gravel-sized material. (B) Two-dimensional planform and cross-section architecture observed from stratigraphic reconstructions and outcrop. Similar geometries and stacking patterns were observed in all datasets and varied based on orientation relative to the flow direction and degree of reworking (see Figs 9A, 10A and 16A). (C) Fence diagram highlighting the 3D architecture of bedform deposits including the shape and orientation of erosional basal bounding surfaces. See Appendix S4 for videos of fence diagram reconstructions showing the 3D stratigraphic evolution of bedform deposits including all perspectives (dip, strike, oblique and planform).

some cases a greater proportion of planar – low-angle, upslope-inclined, often diffuse stratified facies are observed either within or at the top of beds (Postma *et al.*, 2014, in press; Ito *et al.*, 2014; Lang *et al.*, 2017; Yang *et al.*, 2017; Ono & Plink-Björklund, 2017; Postma & Kleverlaan, 2018; Cornard & Pickering, 2019). Recent work has questioned some of the process-facies linkages in classic turbidite models and proposed new associations, including top-cut-out units containing structureless Bouma (1962) Ta divisions with soft sediment deformation and stratified Tb divisions (Tb4 to Tb2), related to deposition on cyclic steps (Postma & Cartigny, 2014). However, predictive facies models may be complicated by variability along cyclic steps, incomplete preservation, the presence and reworking of unrelated mass-wasting deposits, and turbidity current characteristics such as flow unsteadiness (for example, eventual waning) and high sediment fallout rates. For example, Hage *et al.* (2018) suggested that the lack of stratification observed in bedform deposits on the Squamish delta may be a result of preferential preservation of hydraulic jump zone deposits and high near-bed sediment concentrations. Thus, facies are variable and often non-unique; they alone are presently not conclusive for recognizing cyclic step deposits in a 1D section such as a core or laterally restricted outcrop. Further investigation is required to determine whether distinct cyclic step facies exist and can reliably differentiate deposition from high-density turbidity currents under different flow conditions.

Scale and stratigraphic architecture

The scale and architecture of deposits in 2D and 3D sections are more diagnostic for recognition and facilitated the identification of cyclic step deposits in the Nanaimo Group (Fig. 17B and C). Successions dominated by beds with overall spoon/flute-shaped geometry, low-angle upslope inclination and backset stacking patterns are associated with cyclic steps in the analyzed datasets (Figs 16A and 17C). These observations are generally consistent with lenticular units and/or backset stratification described in flume experiments (Ono *et al.*, 2019; Yokokawa *et al.*, 2009; Cartigny *et al.*, 2014; Fedele *et al.*, 2016) as well as numerical and conceptual models of cyclic steps (Kostic, 2011; Postma *et al.*, 2014; Vellinga *et al.*, 2018; Slootman & Cartigny, 2020). Comparable architecture (asymmetrical scours and backset beds that thicken upslope)

and surface dip angles have also been observed and attributed to cyclic steps in other deep-water outcrop investigations (Postma *et al.*, 2014, in press; Ito *et al.*, 2014; Gong *et al.*, 2017; Lang *et al.*, 2017; Yang *et al.*, 2017; Ono & Plink-Björklund, 2017; Postma & Kleverlaan, 2018; Cornard & Pickering, 2019). However, some deposit characteristics vary between studies, such as the scale of structures in terms of their length/height (ranging from decimetres to tens of metres long/centimetres to metres tall) and thickness of stratification (lamination – bed scale), the nature and continuity of bed boundaries, and the prevalence of the described features (i.e. isolated or dominant in a succession).

Several factors can influence the geometry and appearance of cyclic step deposits. Bedform deposit dimensions generally relate to the morphology of associated bedforms. However, scaling relationships may be ambiguous because bedform deposit size also depends on the degree of subsequent erosion (Fig. 8; Yokokawa *et al.*, 2009; Vellinga *et al.*, 2018; Slootman & Cartigny, 2020). Similar observations have been made for sedimentary structures associated with ripples and dunes where cross-set thickness is related to both aggradation rate and bedwave height distribution (Bridge, 1997; Leclair *et al.*, 1997). Several studies have identified aggradation rate as the main controlling factor on cyclic step deposit architecture (Fig. 1F; Hage *et al.*, 2018; Vellinga *et al.*, 2018; Slootman & Cartigny, 2020). Moreover, recent flume experiments by Ono *et al.* (2019) demonstrate that hydraulic jump size, stability and migration rate as well as grain-size distribution are also important. Experiments reveal complex, variable successions produced by cyclic step hydraulic jump dynamics under overall constant flow conditions, which share characteristics with the deposits of other upper-flow-regime and lower-flow-regime bedforms (Ono *et al.*, 2019).

The stratigraphic products of cyclic step bedforms (10 to 140 m wavelengths, <10 m wave heights) formed by the passage of multiple turbidity currents with mixed sediment loads (including mud – gravel grain sizes), under low-aggradation conditions are captured in this study (Figs 5A, 16 and 17). Repeat bathymetry surveys from the Squamish prodelta indicate stable, periodic hydraulic jump upslope-migration during flow events (for example, Figs 2D and 6), whereas the nature of hydraulic jumps in the upper Monterey Canyon is unclear and may be more irregular.

Stratigraphic reconstructions suggest that in these cases, stratification may occur at the bed scale (i.e. decimetre scale) where between-flow-unsteadiness results in nested, sharply bounded beds, which are subtly offset upslope (Figs 9A, 10A, 16A, 17B and 17C). Although deposit variability exists, asymmetrical geometry and local backset stratification is evident and diagnostic in each succession. It may be more difficult to recognize cyclic step deposits in 2D strike-oriented outcrops where backset bedding is not apparent (Figs 9A, 10A, 17B and 17C). In addition, as exemplified in the upper Monterey canyon dataset, inconsistent and more diverse deposit geometry and stratification may result due to greater erosion and reduced preservation (Vellinga *et al.*, 2018), or the potential occurrence of small and/or unstable hydraulic jumps (Fig. 10, Ono *et al.*, 2019).

When considered as a whole, the cyclic step successions documented here are distinct from the products expected from lower-flow-regime bedforms, which are dominated by consistent foreset stratification and preservation of steeper lee slopes (Fig. 17; Slootman & Cartigny, 2020). However, it is less clear whether other upper-flow-regime bedforms (for example, antidunes), which may also be relatively long-lived (West *et al.*, 2019), could have comparable depositional signatures in deep-water settings. In addition, the identified recognition criteria may not be valid for all styles of cyclic steps as variability in aggradation rate, hydraulic jump dynamics, flow characteristics, sediment calibre and bedform longevity may result in different stratigraphic expressions.

Implications for palaeoenvironmental reconstructions

Palaeoflow conditions

Bedform deposits are important for palaeoenvironmental interpretations and can preserve morphometric information useful for reconstructing the nature and evolution of sediment transport from ancient successions (Allen, 1982; Best & Bridge, 1992; Bridge, 1997; Leclair *et al.*, 1997; Alexander *et al.*, 2001; Jobe *et al.*, 2012; Cartigny *et al.*, 2014). The presence and architecture of Nanaimo Group deposits exposed around the Twin Beaches Peninsula suggest that the succession formed under supercritical flow conditions in a fluctuating but overall low aggradation regime, such as that found in channels of the Squamish prodelta and Upper Monterey Canyon (Figs 7C and 16A).

The dimensions of bedforms in the modern study areas and bedform deposits in all three locations are also relatively consistent (Fig. 16). The scale of deposits is important for directly tying features in the rock record to bedforms observed on the seafloor and their associated flow characteristics. Thus, the slightly smaller bedform deposits observed at the Twin Beaches Peninsula compared to those in modern reconstructions (Fig. 16) could reflect: smaller formative bedforms due to slight differences in slope gradient or flow characteristics (Cartigny *et al.*, 2011; Kostic, 2011; Fricke *et al.*, 2015; Normandeau *et al.*, 2016; Slootman & Cartigny, 2020); more extensive reworking (Hage *et al.*, 2018; Vellinga *et al.*, 2018; Vendettuoli *et al.*, 2019); or a bias related to comparing outcrop and bathymetry datasets. The longer timescales involved in ancient deposits enhance the likelihood of encompassing large, extreme events which could affect the size and preservation of deposits (Miall, 2015). In addition, both datasets include uncertainties related to differentiating individual event beds, which could affect deposit size distribution. Deposits reconstructed from bathymetry datasets are likely composite and consist of unrecognized, smaller geometries due to the occurrence of multiple flows between two surveys, while bed amalgamation can make individual units difficult to delineate in outcrop.

The similar scale of seafloor bedforms and bedform deposits in the investigated areas is likely related to properties of flows that can occur in multiple turbidity-current-dominated environments and water depths. Observations of flows in Squamish prodelta channels and Monterey Canyon, although not from the exact location of the bathymetric surveys used in this study, are characterized by turbidity currents with relatively fast, thin and dense basal layers (1 to 3 m thick, reaching 1 to 5 m s^{-1} velocities) that interact with bedforms (Fig. 5B; Postma *et al.*, 1988; Sohn, 1997; Hughes Clarke, 2016; Jobe *et al.*, 2017; Paull *et al.*, 2018; Wang *et al.*, 2020). Similar flow characteristics have been previously associated with other relatively small-scale, coarse-grained, upslope-migrating bedforms based on numerical and conceptual models of cyclic steps (Cartigny *et al.*, 2011; Postma & Cartigny, 2014; Symons *et al.*, 2016). Thus it is likely that energetic, stratified, high-density flows are ubiquitously responsible for bedforms of this type and also formed the bedform deposits of the Cretaceous Gabriola Formation.

Palaeoflow direction

Bedform deposits are not only significant for providing insight into flow and sediment transport conditions, but their associated stratification can be used to reconstruct palaeoflow direction (Allen, 1982; Rubin, 1987). Typically this stratification occurs at the scale of laminations or thin beds, which form sets bound by larger bedding surfaces (Allen, 1982). In the cyclic step deposits described here, low-angle stratification occurs within medium to very thick beds where smaller-scale internal stratification is absent, crude or variably oriented. In addition to potentially long length scales, these factors make the precise determination of palaeoflow direction from stratification alone more challenging.

Palaeoflow directions can be directly constrained by measuring the orientation of the basal surface of trough-shaped deposits, as shown in the modern systems (Figs 9, 10, 17B and 17C). However, in order to do this effectively, it is important to identify the component of the 3D surface (upslope/foreset, edge or downslope/backset portion) being measured. This can be accomplished by determining the general outcrop orientation relative to the palaeoflow direction either by: independent measurements of other nearby palaeoflow indicators (for example, ripple foresets and sole marks); or examination of overall deposit architecture where subtleties in individual deposit geometry, proportions and stacking can differentiate depositional dip and strike-oriented sections (Fig. 17B and 17C). The measured strike, down-dip and up-dip direction of edge, foreset and backset surfaces, respectively, can then be used as the palaeoflow direction. Backsets tend to have overall low dips (<10°), which may be difficult to measure in the field and be particularly sensitive to structural tilting (Fig. 16A). However, stepped or undulatory segments can provide locally steeper surface measurements (Fig. 13; Ono *et al.*, 2019; Spinewine *et al.*, 2009; Yokokawa *et al.*, 2009; Cartigny *et al.*, 2011). Interpretation of palaeoflow direction based on strike and dip measurements from the basal surfaces of the Nanaimo Group deposits were consistent with palaeoflow determined by measurement of other features (for example, ripple foresets; Fig. 14B).

Modern to Ancient comparisons in deep-water settings

The inaccessibility of modern deep-water environments has previously limited direct observations of deep-water sedimentary processes, and thus the ability to create and validate turbidite depositional models (Talling *et al.*, 2015). This study demonstrates how integrated seafloor datasets, including repeat bathymetry, flow monitoring and sediment coring, can be leveraged to improve understanding of deep-water stratigraphy by providing new inspiration for evaluating and informing interpretations of the sedimentary record. These comparisons allow direct linkages to be established between bedforms produced by naturally-occurring turbidity currents and sedimentary structures observed in the rock record, in this case providing robust support for positive identification of cyclic steps in deep-water strata.

Differences in the spatial and temporal resolution of datasets make the comparison of modern and ancient settings difficult but also complementary (Mutti & Normark, 1987). Modern investigations can only detect features above the resolution limits of imaging techniques (typically >1.0 m horizontal, >0.1 m vertical) and monitor processes that operate over short time-scales (on the order of days to years). Integrated seafloor datasets including repeat monitoring and surveying are presently biased towards sandy, shallow environments (<250 m water depth) where high resolution imaging is more accessible and flow events occur more frequently (sub-annually); however, it is uncertain how these observations extend to deeper-water, mud-rich systems and longer timescales (Talling *et al.*, 2015; Vendettuoli *et al.*, 2019). For example, roughness calculations from the deep-water, muddy Congo Canyon suggest an absence of bedforms (Simmons *et al.*, 2020). On the other hand, outcrop investigations can capture smaller features (typically at centimetre to metre scale) that represent longer term perspectives (thousands to millions of years) but are biased by incomplete preservation and limited context.

Between seafloor and outcrop investigations, upper-flow-regime bedforms have been reported spanning a wide range of sizes, on the order of centimetres to kilometres (e.g. Postma *et al.*, 2014; Symons *et al.*, 2016; Lang *et al.*, 2017; Cornard & Pickering, 2019). Although similar processes may operate at different spatial and temporal scales (Fig. 1A), it is important to consider compatibility in terms of size and duration before making direct modern to ancient comparisons. Study area and data acquisition limitations still inhibit the identification of 100 to 1000 m scale bedform features (for example large-scale sediment waves and large-scale

scours; Fig. 1A) in most outcrops, while smaller features often observed in outcrop are not resolvable on the seafloor (Mutti & Normark, 1991). This study features cyclic steps, morphologically equivalent to small-scale sediment waves, and their associated sedimentary structures at an intermediate scale (on the order of metres to tens of metres; Fig. 1A). Modern study areas capture flow conditions and low net accumulation over surveyed time periods while identification in the Nanaimo Group succession demonstrates that preservation can occur over geological timescales and at greater water depths.

Although cyclic steps are not present in all modern deep-water systems and their deposits have been reported from some deep-water outcrops (e.g. Postma *et al.*, 2014; Lang *et al.*, 2017; Cornard & Pickering, 2019), bedforms are much more widely identified on the seafloor than their sedimentary structures documented in deep-water successions. Under-representation in the rock record could be a result of insufficient recognition or, in some cases, recognition may not be possible due to indistinct stratigraphic products (for example, large deposits, uniform grain-size distributions and non-unique facies). The apparent discrepancy in cyclic step deposit occurrence may also be related to bedform preservation, which may be poor (as observed in the Squamish prodelta and upper Monterey Canyon), and ultimately only favoured under specific conditions and/or in certain depositional environments. Additionally the role of bedforms in larger infrequent events, which deposit or flush large volumes of sediment in channels and have the largest impact on the stratigraphic record (cf. Mountjoy *et al.*, 2018; Vendettuoli *et al.*, 2019), is at present poorly constrained.

CONCLUSION

Repeat bathymetric surveys from two modern environments (Squamish prodelta, British Columbia and Monterey Canyon, California) establish process to product relationships for macro-scale upslope-migrating bedforms (<300 m wavelength, <8 m wave heights) interpreted as cyclic steps. Quantitative comparisons of reconstructed bedform deposits from these datasets are used to inform interpretations of cyclic steps in a Late Cretaceous (Nanaimo Group) deep-water succession exposed on Gabriola Island, Canada. Bedform deposits from the two modern systems and ancient outcrop strata are similar in scale, facies and depositional architecture, with each characterized by low-angle backstepping, trough-shaped lenses, which are typically tens of metres long/wide, <1 m thick and composed of massive sands/sandstone. The identification of comparable deposits in prodelta channel, upper canyon and deep-water slope channel environments supports process-based relationships associated with low-aggradation cyclic steps (on average 40 to 55 m wavelengths, 1.5 to 3.0 m wave heights, 39 to 74% deposit reworking). Bedforms of similar size and morphology are found abundantly in coarse-grained turbidite-dominated environments. Thus, this dataset may represent typical bedform deposit dimensions and geometries that form beneath turbidity currents with dense basal layers 1 to 4 m thick and 1 to 5 m s^{-1} flow velocities under low-aggradation conditions.

The scale and three-dimensional architecture of deposits are key criteria for identification of the bedform deposits in outcrop, while facies alone are non-unique in the examined datasets. For cyclic steps that persist over multiple flow events, backset stratification develops at the bed-scale where between-flow-unsteadiness and low-aggradation result in nested, erosion-surface-bound units. Deposit architecture and stacking is useful for determining the general palaeoflow direction while more precise directions can be obtained by appropriately measuring the orientation of foreset, backset and/or edge components of basal bounding surfaces. More work is clearly required to establish recognition criteria and understand process to product relationships for the wide variety of seafloor bedforms, as well as sedimentary structures documented in the rock record. Integration of novel seafloor datasets provides added insight into palaeoenvironmental interpretations of deep-water stratigraphy that in turn can fill gaps in current understanding of seafloor processes, such as the extent to which processes operate in deeper environments and over longer timescales.

ACKNOWLEDGEMENTS

DATA AVAILABILITY STATEMENT

The data that supports the findings of this study are available in the supporting information of this article. The Monterey bathymetry data were derived from the following resource available in the public domain (Seafloor Mapping Lab): https://seafloor.otterlabs.org/.

REFERENCES

Alexander, J., **Bridge, J.S.**, **Cheela, R.J.** and **Leclair, S.F.** (2001) Bedforms and associated sedimentary structures formed under supercritical waterflows over aggrading sand beds. *Sedimentology*, **48**, 133–152.

Allen, J.R.L. (1982) *Sedimentary Structures: Their Character and Physical Basis*, vol. **I**. Elsevier, Amsterdam, 593 pp.

Azpiroz-Zabala, M., **Cartigny, M.J.B.**, **Talling, P.J.**, **Parsons, D.R.**, **Sumner, E.J.**, **Clare, M.A.**, **Simmons, S.M.**, **Cooper, C.** and **Pope, E.** (2017) Newly recognized turbidity current structure can explain prolonged flushing of submarine canyons. *Sci. Adv.*, **3**, e1700200.

Babonneau, N., **Delacourt, C.**, **Cancouët, R.**, **Sisavath, E.**, **Bachèlery, P.**, **Mazuel, A.**, **Jorry, S.J.**, **Deschamps, A.**, **Ammann, J.** and **Villeneuve, N.** (2013) Direct sediment transfer from land to deep-sea: insights into shallow multibeam bathymetry at La Réunion Island. *Mar. Geol.*, **346**, 47–57.

Bain, H.A. and **Hubbard, S.M.** (2016) Stratigraphic evolution of a long-lived submarine channel system in the Late Cretaceous Nanaimo Group, British Columbia, Canada. *Sed. Geol.*, **337**, 113–132.

Best, J.L. and **Bridge, J.S.** (1992) The morphology and dynamics of low amplitude bedwaves upon upper stage plane beds and the preservation of planar lamination. *Sedimentology*, **39**, 737–752.

Best, T.C. and **Griggs, G.B.** (1991) A sediment budget of the Santa Cruz littoral cell. In: *From shoreline to abyss: contributions in marine geology in honor of Francis Parker Shepard* (Ed. Osbourne, R.H.), *SPEM Spec. Pub.*, **46**, 35–50.

Bouma, A.H. (1962) *Sedimentology of some Flysch Deposits: A Graphic Approach to Facies Interpretation*. Elsevier, Amsterdam, 168 pp.

Bridge, J.S. (1997) Thickness of sets of cross strata and planar strata as a function of formative bed-wave geometry and migration, and aggradation rate. *Geology*, **25**, 971–974.

Brooks, H.L., **Hodgson, D.M.**, **Brunt, R.L.**, **Peakall, J.**, **Hofstra, M.** and **Flint, S.S.** (2018) Deep-water channel-lobe transition zone dynamics: processes and depositional architecture, an example from the Karoo Basin, South Africa. *Geol. Soc. Am. Bull.*, **130**, 1723–1746.

Cartigny, M.J.B., **Postma, G.**, **Van den Berg, J.H.** and **Mastbergen, D.R.** (2011) A comparative study of sediment waves and cyclic steps based on geometries, internal structures and numerical modelling. *Mar. Geol.*, **280**, 40–56.

Cartigny, M.J.B., **Ventra, D.**, **Postma, G.** and **Van den Berg, J.H.** (2014) Morphodynamics and internal structures of bedforms under supercritical-flow conditions. *Sedimentology*, **61**, 712–748.

Carvajal, C., **Paull, C.K.**, **Caress, D.W.**, **Fildani, A.**, **Lundsten, E.**, **Anderson, K.**, **Maier, K.L.**, **McGann, M.**, **Gwiazda, R.** and **Herguera, J.C.** (2017) Unraveling the channel-lobe transition zone with high-resolution AUV bathymetry: Navy fan, offshore Baja California, Mexico. *J. Sed. Res.*, **87**, 1049–1059.

Casalbore, D., **Clare, M.A.**, **Pope, E.L.**, **Quartau, R.**, **Bosman, A.**, **Chiocci, F.L.**, **Romagnoli, C.** and **Santos, R.** (in press) Bedforms on the submarine flanks of insular volcanoes: New insights gained from high resolution seafloor surveys. *Sedimentology*. https://doi.org/10.1111/sed.12725

Castelltort, S., **Honegger, L.**, **Adatte, T.**, **Clark, J.**, **Puigdefàbregas, C.**, **Spangenber, J.E.**, **Dykstra, M.L.** and **Fildani, A.** (2017) Detecting eustatic and tectonic signals with carbon isotopes in deep-marine strata, Eocene Ainsa Basin, Spanish Pyrenees. *Geology*, **48**, 707–710.

Clare, M.A., **Talling, P.J.** and **Hunt, J.** (2015) Implications of reduced turbidity current and landslide activity for the Initial Eocene Thermal Maximum – evidence from two distal, deep-water sites. *Earth Planet. Sci. Lett.*, **420**, 102–115.

Clare, M.A., **Hughes Clarke, J.E.**, **Talling, P.J.**, **Cartigny, M.J.** and **Pratomo, D.G.** (2016) Preconditioning and triggering of offshore slope failures and turbidity currents revealed by most detailed monitoring yet at a fjord-head delta. *Earth Planet. Sci. Lett.*, **450**, 208–220.

Clare, M.A., **Vardy, M.E.**, **Cartigny, M.J.B.**, **Talling, P.J.**, **Himsworth, M.D.**, **Dix, J.K.**, **Harris, J.M.**, **Whitehouse, R.J.S.** and **Belal, M.** (2017) Direct monitoring of active geohazards: emerging geophysical tools for deep-water assessments. *Near Surf. Geophys.*, **15**, 427–444.

Clare, M.A., **Lintern, D.G.**, **Rosenberger, K.**, **Hughes Clarke, J.E.**, **Paull, C.**, **Gwiazda, R.**, **Cartigny, M.J.B.**, **Talling, P.J.**, **Perara, D.**, **Xu, J.**, **Parsons, D.**, **Silva Jacinto, R.** and **Apprioual, R.** (2020) Lessons learned from monitoring turbidity currents and guidance for future platform designs. *Geol. Soc., London, Spec. Publ.*, **500**, 605–634. https://doi.org/10.1144/SP500-2019-173

Clift, P.D. (2006) Controls on the erosion of Cenozoic Asia and the flux of clastic sediment to the ocean. *Earth Planet. Sci. Lett.*, **241**, 571–580.

Cornard, P.H. and **Pickering, K.T.** (2019) Supercritical-flow deposits and their distribution in a submarine channel system, middle Eocene, Ainsa basin, Spanish Pyrenees. *J. Sed. Res.*, **89**, 576–597.

Covault, J.A., **Kostic, S.**, **Paull, C.K.**, **Sylvester, Z.** and **Fildani, A.** (2017) Cyclic steps and related supercritical bedforms: building blocks of deep-water depositional systems, western North America. *Mar. Geol.*, **393**, 4–20.

Daniels, B.G., **Auchter, N.C.**, **Hubbard, S.M.**, **Romans, B.W.**, **Matthews, W.A.** and **Stright, L.** (2018) The timing of deepwater slope evolutionary phases constrained by large-n detrital and volcanic ash zircon geochronology, Cretaceous Magallanes Basin, Chile. *Geol. Soc. Am. Bull.*, **130**, 438–454.

Eittreim, S.L., **Xu, J.P.**, **Noble, M.** and **Edwards, B.D.** (2002) Towards a sediment budget for the Santa Cruz shelf. *Mar. Geol.*, **181**, 235–248.

England, T.D.J. and **Hiscott, R.N.** (1992) Lithostratigraphy and deep-water setting of the upper Nanaimo Group (Upper Cretaceous), outer Gulf Islands of southwestern British Columbia. *Can. J. Earth Sci.*, **29**, 564–595.

Englert, R.G., **Hubbard, S.M.**, **Coutts, D.S.** and **Matthews, W.A.** (2018) Tectonically controlled initiation of contemporaneous deep-water channel systems along a Late Cretaceous continental margin, western British Columbia Canada. *Sedimentology*, **65**, 2404–2438.

Englert, R.G., **Hubbard, S.M.**, **Matthews, W.A.**, **Coutts, D.S.** and **Covault, J.A.** (2020) The evolution of submarine slope channel systems: timing of incision, bypass, and aggradation in Late Cretaceous Nanaimo Group channel system strata, BC, Canada. *Geosphere*, **16**, 281–296.

Fedele, J.J., **Hoyal, D.**, **Barnaal, Z.**, **Tulenko, J.** and **Awatt, S.** (2016) Bedforms created by gravity flows. In: *Autogenic Dynamics and Self-organization in Sedimentary Systems* (Eds Budd, D.A., Hajek, E.A. and Purkis, S.J.), *SEPM Spec. Publ.*, **106**, 95–121.

Fildani, A., **Kostic, S.**, **Covault, J.A.**, **Maier, K.L.**, **Caress, D.W.** and **Paull, C.K.** (in press) Exploring supercritical bedforms of distal submarine fans. *Sedimentology*.

Fildani, A., **Normark, W.R.**, **Kostic, S.** and **Parker, G.** (2006) Channel formation by flow stripping: large-scale scour features along the Monterey East Channel and their relation to sediment waves. *Sedimentology*, **53**, 1265–1287.

Fildani, A., **Hessler, A.M.**, **Mason, C.**, **McKay, M.P.** and **Stockli, D.F.** (2018) Late Pleistocene glacial transitions in North America altered major river drainages, as revealed by deep-sea sediment. *Sci. Rep.*, **8**, 13839.

Fricke, A.T., **Sheets, B.A.**, **Nittrouer, C.A.**, **Allison, M.A.** and **Ogston, A.S.** (2015) An examination of froude-supercritical flows and cyclic steps on a subaqueous Lacustrine Delta, Lake Chelan, Washington, U.S.A. *J. Sed. Res.*, **85**, 754–767.

Gales, J.A., **Talling, P.J.**, **Cartigny, M.J.B.**, **Hughes Clarke, J.**, **Lintern, G.**, **Stacey, C.** and **Clare, M.A.** (2019) What controls submarine channel development and the morphology of deltas entering deep-water fjords? *Earth Surf. Proc. Land.*, **44**, 535–551.

Gardner, M.H., **Borer, J.M.**, **Melick, J.J.**, **Mavilla, N.**, **Dechesne, M.** and **Wagerle, R.N.** (2003) Stratigraphic process-response model for submarine channels and related features from studies of Permian Brushy Canyon outcrops. *West Texas Mar. Petrol. Geol.*, **20**, 757–787.

Gardner, J.V., **Armstrong, A.A.** and **Calder, B.R.** (2016) Hatteras Transverse Canyon, Hatteras Outer Ridge and environs of the US Atlantic margin: a view from multibeam bathymetry and backscatter. *Mar. Geol.*, **371**, 18–32.

Goldfinger, C. (2011) Submarine paleoseismology based on turbidite records. *Annu. Rev. Mar. Sci.*, **3**, 35–66.

Gong, C., **Chen, L.** and **West, L.** (2017) Asymmetrical, inversely graded, upstream-migrating cyclic steps in marine settings: late Miocene-early Pliocene Fish Creek-Vallecito Basin, southern California. *Sed. Geol.*, **360**, 35–46.

Greene, H.G. (1977) Geology of the Monterey Bay Region. U.S. Geological Survey Open-File Report 77–718, 371 pp., 9 plates.

Guilocheau, F., **Quéméner, J.-M.**, **Robin, C.**, **Joseph, P.** and **Broucke, O.** (2004) Genetic units/parasequences of the Annot turbidite system, SE France. In: *Deep-water sedimentation in the Alpine Basin of SE France: New perspectives on the Grès d'Annot and related systems* (Eds Joseph, P. and Lomas, S.A.), *Geol. Soc. London Spec. Pub.*, **221**, 181–202.

Hage, S., **Cartigny, M.J.B.**, **Clare, M.A.**, **Sumner, E.J.**, **Vendettuoli, D.**, **Hughes Clarke, J.E.**, **Hubbard, S.**, **Talling, P.J.**, **Lintern, D.G.**, **Stacey, C.D.**, **Englert, R.G.**, **Vardy, M.E.**, **Hunt, J.E.**, **Yokokawa, M.**, **Parsons, D.R.**, **Hizzett, J.L.**, **Azpiroz- Zabala, M.** and **Vellinga, A.J.** (2018) How to recognize crescentic bedforms formed by supercritical turbidity currents in the rock record: insights from active submarine channels. *Geology*, **46**, 563–566.

Hage, S., **Cartigny, M.J.B.**, **Sumner, E.J.**, **Clare, M.A.**, **Hughes Clarke, J.E.**, **Talling, P.J.**, **Lintern, D.G.**, **Simmons, S.M.**, **Silva Jacinto, R.**, **Vellinga, A.J.**, **Allin, J.R.**, **Azpiroz-Zabala, M.**, **Gales, J.A.**, **Hizzett, J.L.**, **Hunt, J.E.**, **Mozzato, A.**, **Parsons, D.R.**, **Pope, E.L.**, **Stacey, C.D.**, **Symons, W.O.**, **Varcy, M.E.** and **Watts, C.** (2019) Direct monitoring reveals initiation of turbidity currents from extremely dilute river plumes. *Geophys. Res. Lett.*, **46**, 310–320.

Hamilton, P.B., **Strom, K.B.** and **Hoyal, D.C.J.D.** (2015) Hydraulic and sediment transport properties of autogenic avulsion cycles on submarine fans with supercritical distributaries. *J. Geophys. Res.*, **120**, 1369–1389.

Haughton, P.D.W., **Davis, C.**, **McCaffrey, W.** and **Barker, S.P.** (2009) Hybrid sediment gravity flow deposits – classification, origin and significance. In: *Hybrid and Transitional Submarine Flows* (Eds Amy, L.A., McCaffrey, W.B. and Talling, P.J.), *Mar. Petrol. Geol.*, **26**, 1900–1918.

Heerema, C.J., **Talling, P.J.**, **Cartigny, M.J.**, **Paull, C.K.**, **Bailey, L.**, **Simmons, S.M.**, **Parsons, D.R.**, **Clare, M.A.**, **Gwiazda, R.**, **Lundsten, E.**, **Anderson, K.**, **Maier, K.L.**, **Xu, J.P.**, **Sumner, E.J.**, **Rosenberger, K.**, **Gales, J.**, **McGann, M.**, **Carter, L.**, **Pope, E.** and **Monterey Coordinated Canyon Experiment (CEE) Team** (2020) What determines the downstream evolution of turbidity currents? *Earth Planet. Sci. Lett.*, **532**, 116023.

Heiniö, P. and **Davies, R.J.** (2009) Trails of depressions and sediment waves along submarine channels on the continental margin of Espirito Santo Basin, Brazil. *Geol. Soc. Am. Bull.*, **121**, 698–711.

Hessler, A.M. and **Fildani, A.** (2019) Deep-sea fans: tapping into Earth's changing landscapes. *J. Sed. Res.*, **89**, 1171–1179.

Hickin, E.J. (1989) Contemporary Squamish River sediment flux to Howe Sound, British Columbia. *Can. J. Earth Sci.*, **26**, 1953–1963.

Hill, P.R. (2012) Changes in submarine channel morphology and slope sedimentation patterns from repeat multibeam surveys in the Fraser River delta, western Canada. In: *Sediments, Morphology and Sedimentary Processes on Continental Shelves* (Eds Li, M.Z., Sherwood, C.R. and Hill, P.R.), *Int. Assoc. Sedimentol. Spec. Publ.*, **44**, 47–70.

Hizzett, J.L., **Hughes Clarke, J.E.**, **Sumner, E.J.**, **Cartigny, M.J.B.**, **Talling, P.J.** and **Clare, M.A.** (2017) Which triggers

produce the most erosive, frequent and longest runout turbidity currents on deltas? *Geophys. Res. Lett.*, **45**, 855–863.

Hodgson, D.M., DiCelma, C.N., Brunt, R.L. and Flint, S.S. (2011) Submarine slope degradation, aggradation and the stratigraphic evolution of channel-levee systems. *J. Geol. Soc. London*, **168**, 625–628.

Hofstra, M., Hodgson, D.M., Peakall, J. and Flint, S.S. (2015) Giant scour-fills in ancient channel-lobe transition zones: formative processes and depositional architecture. *Sediment. Geol.*, **329**, 98–114.

Hughes Clark, J.E., Videra Marques, C.R. and Pratomo, D. (2014) Imaging active mass wasting on a fjord delta, Squamish, British Columbia. In: *Submarine Mass Movements and Their Consequences VI* (Eds Krastel, S., Behrmann, J.-H., Volker, D., Stipp, M., Berndt, C., Urgeles, R., Chaytor, J.D., Huhn, K., Stasser, M. and Harbitz, C.B.), Springer, *Advances in Natural and Technological Hazards Research*, **37**, 249–260.

Hughes Clarke, J.H. (2016) First wide-angle view of turbidity currents links migrating cyclic steps to flow characteristics. *Nat. Commun.*, **7**, 11896.

Hughes Clarke, J.E., Brucker, S., Muggah, J., Church, I., Cartwright, D., Kuus, P., Hamilton, T., Pratomo, D. and Eisan, B. (2012a) The Squamish ProDelta: Monitoring Active Landslides and Turbidity Currents. Canadian Hydrographic Conference 2012, Proceedings, 15 pp.

Hughes Clarke, J.E., Brucker, S., Muggah, J., Hamilton, T., Cartwright, D., Church, I. and Kuus, P. (2012b) Temporal progression and spatial extent of mass wasting events on the Squamish prodelta slope. In: *Landslides and Engineered Slopes: Protecting Society Through Improved Understanding* (Eds Eberhardt, E., Froese, C., Turner, K. and Leroueil, S.), pp. 1091–1096. Taylor & Francis Group, London.

Ito, M., Ishikawa, K. and Nishida, N. (2014) Distinctive erosional and depositional structures formed at a canyon mouth: a lower Pleistocene deep-water succession in the Kazusa forearc basin on the Boso Peninsula, Japan. *Sedimentology*, **61**, 2042–2062.

Jobe, Z.R., Lowe, D.R. and Morris, W.R. (2012) Climbing-ripple successions in turbidite systems: depositional environments, sedimentation rates and accumulation times. *Sedimentology*, **59**, 867–898.

Jobe, Z.R., Sylvester, Z., Bolla Pittaluga, M., Frascati, A., Pirmez, C., Minisini, D., Howes, N. and Cantelli, A. (2017) Facies architecture of submarine channel deposits on the western Niger Delta slope: implications for grain-size and density stratification in turbidity currents. *J. Geophys. Res. Earth Surf.*, **122**, 473–491.

Jobe, Z.R., Howes, N., Romans, B.W. and Covault, J.A. (2018) Volume and recurrence of submarine-fan-building turbidity currents. *Depositional Rec.*, **4**, 160–176.

Kane, I.A., Clare, M.A., Miramontes, E., Wogelius, R., Rothwell, J.J., Garreau, P. and Pohl, F. (2020) Seafloor microplastic hotspots controlled by deep-sea circulation. *Science*, **368**, 1140–1145.

Katnick, D.C. and Mustard, P.S. (2003) Geology of Denman and Hornby islands, British Columbia: implications for Nanaimo Basin evolution and formal definition of the Geoffrey and Spray formations, Upper Cretaceous Nanaimo Group. *Can. J. Earth Sci.*, **40**, 375–393.

Khripounoff, A., Vangriesheim, A., Babonneau, N., Crassous, P., Dennielou, B. and Savoye, B. (2003) Direct observation of intense turbidity current activity in the Zaire Submarine Valley at 4000 m water depth. *Mar. Geol.*, **194**, 151–158.

Kostic, S. (2011) Modeling of submarine cyclic steps: controls on their formation, migration, and architecture. *Geosphere*, **7**, 294–304.

Kostic, S. and Parker, G. (2006) The response of turbidity currents to a canyon–fan transition: internal hydraulic jumps and depositional signatures. *J. Hydraul. Res.*, **44**, 631–653.

Lamb, M.P., Parson, J.D., Mullenbach, B.L., Finalyson, D.P., Orange, D.L. and Nittrouer, C.A. (2008) Evidence for superelevation, channel incision, and formation of cyclic steps by turbidity currents in Eel Canyon, California. *Geol. Soc. Am. Bull.*, **120**, 463–475.

Lang, J., Brandes, C. and Winsemann, J. (2017) Erosion and deposition by supercritical density flows during channel avulsion and backfilling: field examples from coarse-grained deep-water channel-levée complexes (Sandino Forearc Basin, southern Central America). *Sed. Geol.*, **349**, 79–102.

Leclair, S.F., Bridge, J.S. and Wang, F. (1997) Preservation of cross-strata due to migration of subaqueous dunes over aggrading and non-aggrading beds: comparison of experimental data with theory. *Geosci. Can.*, **24**, 55–66.

Lowe, D.R. (1982) Sediment gravity flows; II, Depositional models with special reference to the deposits of high-density turbidity currents. *J. Sed. Res.*, **52**, 279–297.

Macauley, R.V. and Hubbard, S.M. (2013) Slope channel sedimentary processes and stratigraphic stacking, Cretaceous Tres Pasos Formation slope system, Chilean Patagonia. *Mar. Petrol. Geol.*, **41**, 146–162.

Macdonald, H.A., Wynn, R.B., Huvenne, V.A., Peakall, J., Masson, D.G., Weaver, P.P. and McPhail, S.D. (2011) New insights into the morphology, fill, and remarkable longevity (>0.2 m.y.) of modern deep-water erosional scours along the northeast Atlantic margin. *Geosphere*, **7**, 845–867.

Maier, K.L., Fildani, A., Paull, C.K., Graham, S.A., McHargue, T.R., Caress, D.W. and McGann, M. (2011) The elusive character of discontinuous deep-water channels: new insights from Lucia Chica, offshore California. *Geology*, **39**, 327–330.

Maier, K.L., Fildani, A., Paull, C.K., McHargue, T.R., Graham, S.A. and Caress, D.W. (2013) Deep-sea channel evolution and stratigraphic architecture from inception to abandonment from high-resolution Autonomous Underwater Vehicle surveys offshore central California. *Sedimentology*, **60**, 935–960.

Maier, K.L., Brothers, D.S., Paull, C.K., McGann, M., Caress, D.W. and Conrad, J.E. (2017) Records of continental slope sediment flow morphodynamic responses to gradient and active faulting from integrated AUV and ROV data, offshore Palos Verdes, southern California Borderland. *Mar. Geol.*, **393**, 47–66.

Maier, K.L., Gales, J.A., Paull, C.K., Rosenberger, K., Talling, P.J., Simmons, S.M., Gwiazda, R., McGann, M., Cartigny, M.J.B., Lundsten, E., Anderson, K., Clare, M.A., Xu, J., Parsons, D., Barry, J.P., Wolfspm-Schwehr, M., Nieminski, N.M. and Sumner, E.J. (2019) Linking direct measurements of turbidity currents to submarine canyon-floor deposits. *Front. Earth Sci.*, **7**, 144.

Maier, K.L., Rosenberger, K.J., Paull, C.K., Gwiazda, R., Gales, J., Lorenson, T., Barry, J.P., Talling, P.J., McGann, M., Xu, J., Lundsten, E., Anderson, K., Litvin, S.Y., Parsons, D.R., Clare, M.A., Simmons, S.M., Sumner, E.J.

and **Cartigny, M.J.B.** (2019b) Sediment and organic carbon transport and deposition driven by internal tides along Monterey Canyon, offshore California. *Deep-Sea Res. Part 1*, **153**, 103108.

Mason, C.C., **Romans, B.W.**, **Stockli, D.F.**, **Mapes, R.W.** and **Fildani, A.** (2019) Detrital zircons reveal sea-level and hydroclimate controls on Amazon River to the deep-sea fan sediment transfer. *Geology*, **47**, 563–566.

Matthews, W.A., **Guest, B.**, **Coutts, D.**, **Bain, H.** and **Hubbard, S.** (2017) Detrital zircons from the Nanaimo basin, Vancouver Island, British Columbia: an independent test of Late Cretaceous to Cenozoic northward translation. *Tectonics*, **36**, 1–23.

Mazières, A., **Gillet, H.**, **Castelle, B.**, **Mulder, T.**, **Guyot, C.**, **Garlan, T.** and **Mallet, C.** (2014) High-resolution morphobathymetric analysis and evolution of Capbreton submarine canyon head (Southeast Bay of Biscay—French Atlantic Coast) over the last decade using descriptive and numerical modeling. *Mar. Geol.*, **351**, 1–12.

McArthur, A., **Kane, I.**, **Bozetti, G.**, **Hansen, L.** and **Kneller, B.C.** (2019) Supercritical flows overspilling from bypass-dominated submarine channels and the development of overbank bedforms. *Depositional Rec.*, **6**, 21–40.

Miall, A.D. (2015) Updating uniformitarianism: stratigraphy as just a set of 'frozen accidents'. *Geol. Soc. Lond. Spec. Publ.*, **404**, 11–36.

Migeon, S., **Savoye, B.**, **Zanella, E.**, **Mulder, T.**, **Faugères, J.C.** and **Weber, O.** (2001) Detailed seismic-reflection and sedimentary study of turbidite sediment waves on the Var Sedimentary Ridge (SE France): significance for sediment transport and deposition and for the mechanisms of sediment-wave construction. *Mar. Petrol. Geol.*, **18**, 179–206.

Mountjoy, J.J., **Howarth, J.D.**, **Orpin, A.R.**, **Barnes, P.M.**, **Bowden, D.A.**, **Rowden, A.A.**, **Schimel, A.C.G.**, **Holden, H.**, **Horgan, H.J.**, **Nodder, S.D.**, **Patton, J.R.**, **Lamarche, G.**, **Gerstenberger, M.**, **Micallef, A.**, **Pallentin, A.** and **Kane, T.** (2018) Earthquakes drive large-scale submarine canyon development and sediment supply to deep-ocean basins. *Sci. Adv.*, **4**, eaar3748.

Mustard, P.S. (1994) The upper cretaceous Nanaimo group, Georgia basin. In: *Geology and Geological Hazards of the Vancouver Region, Southwestern British Columbia* (Ed. Monger, J.W.H.), *Geol. Surv. Can. Bull.*, **481**, 27–95.

Mutti, E. and **Normark, W.R.** (1987) Comparing examples of modern and ancient turbidite systems: problems and concepts. In: *Marine Clastic Sedimentology; Concepts and Case Studies* (Eds Leggett, J.K. and Zuffa, G.G.), pp. 1–38. Graham and Trotman, London.

Mutti, E. and **Normark, W.** (1991) An integrated approach to the study of turbidite systems. In: *Seismic Facies and Sedimentary Processes of Submarine Fans and Turbidite Systems, Ch 4.* (Eds Link, M.H. and Weimer, P.), pp. 75–106. Springer Verlag Inc., New York.

Nesbit, P.R., **Durkin, P.R.**, **Hugenholtz, C.H.**, **Hubbard, S.M.** and **Kucharczyk, M.** (2018) 3-D stratigraphic mapping using a digital outcrop model derived from UAV images and structure-from-motion photogrammetry. *Geosphere*, **14**, 2469–2486.

Normandeau, A., **Lajeunesse, P.**, **Poiré, A.G.** and **Francus, P.** (2016) Morphological expression of bedforms formed by supercritical sediment density flows on four fjord-lake deltas of the south-eastern Canadian Shield (Eastern Canada). *Sedimentology*, **63**, 2106–2129.

Normandeau, A., **Campbell, D.C.** and **Cartigny, M.J.B.** (2019a) The influence of turbidity currents and contour currents on the distribution of deep-water sediment waves offshore eastern Canada. *Sedimentology*, **66**, 1746–1767.

Normandeau, A., **Dietrich, P.**, **Hughes Clarke, J.**, **Van Wychen, W.**, **Lajeunesse, P.**, **Burgess, D.** and **Ghienne, J.-F.** (2019b) Retreat pattern of glaciers controls the occurrence of turbidity currents on high-latitude fjord deltas (Eastern Baffin Island). *J. Geophys. Res. Earth Surf.*, **124**, 1559–1571.

Normark, W.R. (1970) Channel piracy on Monterey Deep-Sea Fan. *Deep-Sea Res.*, **17**, 837–846.

Normark, W.R., **Posamentier, H.** and **Mutti, E.** (1993) Turbidite systems: state of the art and future directions. *Rev. Geophys.*, **31**, 91–116.

Ono, K. and **Plink-Björklund, P.** (2017) Froude supercritical flow bedforms in deepwater slope channels? Field examples in conglomerates, sandstones and fine-grained deposits. *Sedimentology*, **65**, 639–669.

Ono, K., **Plink-Björklund, P.**, **Eggenhuisen, J.T.** and **Cartigny, M.J.B.** (2019) Froude supercritical flow processes and sedimentary structures: new insights from experiments with a wide range of grain sizes. *Sedimentology*. https://doi.org/10.1111/sed.12682

Parker, G. (1996) Some speculations on the relation between channel morphology and channel-scale flow structures. In: *Coherent Flow Structures in Open Channels* (Eds Ashworth, P.J., Bennett, S.J., Best, J.L. and McLelland, S.J.), pp. 423–458. John Wiley & sons, New York.

Paull, C.K., **Ussler III, W.**, **Greene, H.G.** and **Keaten, R.** (2003) Caught in the act: the 20 December 2001 gravity flow event in Monterey Canyon. *Geo.-Mar. Lett.*, **22**, 227–232.

Paull, C.K., **Mitts, P.**, **Ussler III, W.**, **Keaten, R.** and **Greene, H.G.** (2005) Trail of sand in upper Monterey Canyon. *Geol. Soc. Am. Bull.*, **117**, 1134–1145.

Paull, C.K., **Ussler III, W.**, **Caress, D.W.**, **Lundsten, E.**, **Barry, J.**, **Covault, J.A.**, **Maier, K.L.**, **Xu, J.** and **Augenstein, S.** (2010) Origins of large crescent-shaped bedforms within the axial channel of Monterey Canyon. *Geosphere*, **6**, 755–774.

Paull, C.K., **Caress, D.W.**, **Ussler, W.**, **Lundsten, E.** and **Meiner- Johnson, M.** (2011) High-resolution bathymetry of the axial channels within Monterey and Soquel submarine canyons, offshore central California. *Geosphere*, **75**, 1077–1101.

Paull, C.K., **Caress, D.W.**, **Lundsten, E.**, **Gwiazda, R.**, **Anderson, K.**, **McGann, M.**, **Conrad, J.**, **Edwards, B.** and **Sumner, E.J.** (2013) Anatomy of the La Jolla Submarine Canyon system; offshore southern California. *Mar. Geol.*, **335**, 16–34.

Paull, C.K., **Talling, P.J.**, **Maier, K.L.**, **Parsons, D.**, **Xu, J.**, **Caress, D.W.**, **Gwiazda, R.**, **Lundsten, E.M.**, **Anderson, K.**, **Barry, J.P.**, **Chaffey, M.**, **O'Reilly, T.**, **Rosenberger, K.J.**, **Gales, J.A.**, **Kieft, B.**, **McGann, M.**, **Simmons, S.M.**, **McCann, M.**, **Sumner, E.J.**, **Clare, M.A.** and **Cartigny, M.J.** (2018) Powerful turbidity currents driven by dense basal layers. *Nat. Commun.*, **9**, 4114.

Pemberton, E.A.L., **Hubbard, S.M.**, **Fildani, A.**, **Romans, B.** and **Stright, L.** (2016) The stratigraphic expression of decreasing confinement along a deep-water sediment routing system: outcrop example from southern Chile. *Geosphere*, **12**, 114–134.

Pettingill, H.S. and **Weimer, P.** (2002) Worldwide deepwater exploration and production. *Lead. Edge*, **21**, 371–376.

Pickering, K.T., **Hodgson, D.M.**, **Platzman, E.**, **Clark, J.D.** and **Stephens, C.** (2001) A new type of bedform produced by backfilling processes in a submarine channel, Late Miocene, Tabernas-Sorbas Basin, SE Spain. *J. Sed. Res.*, **71**, 692–704.

Piper, D.J.W. and **Kontopoulos, N.** (1994) Bedforms in submarine channels: comparison of ancient examples from Greece with studies of recent turbidite systems. *J. Sed. Res.*, **64**, 247–252.

Piper, D.J.W. and **Savoye, B.** (1993) Processes of late Quaternary turbidity current flow and deposition on the Var deep-sea fan, north-west Mediterranean Sea. *Sedimentology*, **40**, 557–583.

Piper, D.J.W., **Shore, A.N.**, **Farre, J.A.**, **O'Connell, S.** and **Jacobi, R.** (1985) Sediment slides and turbidity currents on the Laurentian Fan: sidescan sonar investigations near the epicentre of the 1929 Grand Banks earthquake. *Geology*, **13**, 538–541.

Pohl, F., **Eggenhuisen, J.T.**, **Kane, I.A.** and **Clare, M.A.** (2020) Transport and burial of microplastics in deep-marine sediments by turbidity currents. *Environ. Sci. Technol.*, **54**, 4180–4189.

Postma, G. and **Cartigny, M.J.** (2014) Supercritical and subcritical turbidity currents and their deposits—a synthesis. *Geology*, **42**, 987–990.

Postma, G. and **Kleverlaan, K.** (2018) Supercritical flows and their control on the architecture and facies of small-radius sand-rich fan lobes. *Sed. Geol.*, **364**, 53–70.

Postma, G., **Lang, J.**, **Hoyal, D.C.**, **Fedele, J.J.**, **Demko, T.**, **Abreu, V.** and **Pederson, K.H.** (in press) Reconstruction of bedform dynamics controlled by supercritical flow in the channel-lobe transition zone of a deep-water delta (Sant Llorenç del Munt, north-east Spain, Eocene). *Sedimentology*. https://doi.org/10.1111/sed.12735

Postma, G., **Nemec, W.** and **Kleinspehn, K.L.** (1988) Large floating clasts in turbidites: a mechanism for their emplacement. *Sed. Geol.*, **58**, 47–61.

Postma, G., **Cartigny, M.** and **Kleverlaan, K.** (2009) Structureless, coarse-tail graded Bouma Ta formed by internal hydraulic jump of the turbidity current? *Sed. Geol.*, **219**, 1–6.

Postma, G., **Kleverlaan, K.** and **Cartigny, M.J.B.** (2014) Recognition of cyclic steps in sandy and gravelly turbidite sequences, and consequences for the Bouma facies model. *Sedimentology*, **61**, 2268–2290.

Prave, A.R. and **Duke, W.L.** (1990) Small-scale hummocky cross-stratification in turbidites: a form of antidune stratification? *Sedimentology*, **37**, 531–539.

Rubin, D.M. (1987) *Cross-bedding, Bedforms, and Paleocurrents. SEPM Concepts in Sedimentology and Paleontology*, SEPM, Tulsa. Vol. **1**. 187 pp.

Seafloor Mapping Lab of California State University Monterey Bay, 2003–2014, Monterey Bay Canyon. https://seafloor.otterlabs.org/

Simmons, S.M., **Azpiroz-Zabala, M.**, **Cartigny, M.J.B.**, **Clare, M.A.**, **Cooper, C.**, **Parsons, D.**, **Pope, E.L.**, **Sumner, E.J.** and **Talling, P.J.** (2020) Novel acoustic method provides first detailed measurements of sediment concentration structure within submarine turbidity currents. *J. Geophys. Res. Oceans*, **125**, e2019JC015904.

Skipper, K. (1971) Antidune cross-stratifcation in a turbidite sequence, Cloridome Formation, Gaspe, Quebec. *Sedimentology*, **17**, 51–68.

Slootman, A. and **Cartigny, M.J.B.** (2020) Cyclic steps: review and aggradation-based classification. *Earth Sci. Rev.*, **201**, 104929.

Smith, D.P., **Ruiz, G.**, **Kvitek, R.** and **Iampietro, P.J.** (2005) Semiannual patterns of erosion and deposition in upper Monterey Canyon from serial multibeam bathymetry. *Geol. Soc. Am. Bull.*, **117**, 1123–1133.

Smith, D.P., **Kvitek, R.**, **Lampietro, P.J.** and **Wong, K.** (2007) Twenty-nine months of geomorphic change in upper Monterey Canyon (2002–2005). *Mar. Geol.*, **236**, 79–94.

Sohn, Y.K. (1997) On traction-carpet sedimentation. *J. Sed. Res.*, **67**, 502–509.

Spinewine, B., **Sequeiros, O.E.**, **Garcia, M.H.**, **Beaubouef, R.T.**, **Sun, T.** and **Savoye, B.** (2009) Experiments on wedge- shaped deep sea sedimentary deposits in minibasins and/or on channel levees emplaced by turbidity currents. Part II. Morphodynamic evolution of the wedge and of the associated bedforms. *J. Sed. Res.*, **79**, 608.

Stacey, C.D., **Hill, P.R.**, **Talling, P.J.**, **Enkin, R.J.**, **Hughes Clarke, J.** and **Lintern, D.G.** (2019) How turbidity current frequency and character varies down a fjord-delta system: combining direct monitoring, deposits and seismic data. *Sedimentology*, **66**, 1–31.

Stevens, T., **Paull, C.K.**, **Ussler III, W.**, **McGann, M.**, **Buylaert, J.-P.** and **Lundsten, E.** (2014) The timing of sediment transport down Monterey Submarine Canyon, offshore California. *Geol. Soc. Am. Bull.*, **126**, 103–121.

Stevenson, C.J., **Jackson, C.A.-L.**, **Hodgson, D.M.**, **Hubbard, S.M.** and **Eggenhuisen, J.T.** (2015) Deep-water sediment bypass. *J. Sed. Res.*, **85**, 1058–1081.

Sumner, E.J. and **Paull, C.K.** (2014) Swept away by a turbidity current in Mendocino submarine canyon, California. *Geophys. Res. Lett.*, **41**, 7611–7618.

Sumner, E.J., **Amy, L.A.** and **Talling, P.J.** (2008) Deposit structure and processes of sand deposition from decelerating sediment suspensions. *J. Sed. Res.*, **78**, 529–547.

Symons, W.O., **Sumner, E.J.**, **Talling, P.J.**, **Cartigny, M.J.B.** and **Clare, M.A.** (2016) Large-scale sediment waves and scours on the modern seafloor and their implications for the prevalence of supercritical flows. *Mar. Geol.*, **371**, 130–148.

Symons, W.O., **Sumner, E.J.**, **Paull, C.K.**, **Cartigny, M.J.B.**, **Xu, J.P.**, **Maier, K.L.**, **Lorenson, T.D.** and **Talling, P.J.** (2017) A new model for turbidity current behavior based on integration of flow monitoring and precision coring in a submarine canyon. *Geology*, **45**, 367–370.

Talling, P.J., **Masson, D.G.**, **Sumner, E.J.** and **Malgesini, G.** (2012) Subaqueous sediment density flows: depositional processes and deposit types. *Sedimentology*, **59**, 1937–2003.

Talling, P.J., **Allin, J.**, **Armitage, D.A.**, **Arnott, R.W.C.**, **Cartigny, M.J.B.**, **Clare, M.A.**, **Felletti, F.**, **Covault, J.A.**, **Girardclos, S.**, **Hansen, E.**, **Hill, P.R.**, **Hiscott, R.N.**, **Hogg, A.J.**, **Hughes Clarke, J.**, **Jobe, Z.R.**, **Malgesini, G.**, **Mozzato, A.**, **Naruse, H.**, **Parkinson, S.**, **Peel, F.J.**, **Piper, D.J.W.**, **Pope, E.**, **Postma, G.**, **Rowley, P.**, **Sguazzini, A.**, **Stevenson, C.J.**, **Sumner, E.J.**, **Sylvester, Z.**, **Watts, C.** and **Xu, J.** (2015) Key future directions for research on turbidity currents and their deposits. *J. Sed. Res.*, **85**, 153–169.

Tripsanas, E.K., **Piper, D.J.W.**, **Jenner, K.A.** and **Bryant, W.R.** (2008) Submarine mass-transport facies: new perspectives on flow processes from cores on the eastern North American margin. *Sedimentology*, **55**, 97–136.

Tubau, X., **Paull, C.K.**, **Lastras, G.**, **Caress, D.W.**, **Canals, M.**, **Lundsten, E.**, **Anderson, K.**, **Gwiazda, R.** and **Amblas, D.** (2015) Submarine canyons of Santa Monica Bay, Southern

California : variability in morphology and sedimentary processes. *Mar. Geol.*, **365**, 61–79.

Vanderkerhove, E., **Bertrand, S.**, **Lanna, E.C.**, **Reid, B.** and **Pantoja, S.** (2020) Modern sedimentary processes at the heads of the Martínez Channel and Steffen Fjord, Chilean Patagonia. *Mar. Geol.*, **416**, 106076.

Vellinga, A.J., **Cartigny, M.J.B.**, **Eggenhuisen, J.T.** and **Hansen, E.W.M.** (2018) Morphodynamics and depositional signature of low-aggradation cyclic steps: new insights from a depth resolved model. *Sedimentology*, **65**, 540–560.

Vendettuoli, D., **Clare, M.A.**, **Hughes Clarke, J.E.**, **Vellinga, A.**, **Hizzet, J.**, **Hage, S.**, **Cartigny, M.J.B.**, **Talling, P.J.**, **Waltham, D.**, **Hubbard, S.M.**, **Stacey, C.** and **Lintern, D.G.** (2019) Daily bathymetric surveys document how stratigraphy is built and its extreme incompleteness in submarine channels. *Earth Planet. Sci. Lett.*, **515**, 231–247.

Walker, R.G. (1967) Upper flow regime bed forms in turbidites of the Hatch formation Devonian of New York State. *J. Sed. Res.*, **37**(4), 1052–1058.

Wang, Z., **Xu, J.**, **Talling, P.J.**, **Cartigny, M.J.**, **Simmons, S.M.**, **Gwiazda, R.**, **Paull, C.K.**, **Maier, K.L.** and **Parsons, D.R.** (2020) Direct evidence of a high-concentration basal layer in a submarine turbidity current. *Deep Sea Res. Part I*, **161**, 103300.

West, L.M., **Perillo, M.M.**, **Olariu, C.** and **Steel, R.J.** (2019) Multi-event organization of deepwater sediments into bedforms: long-lived, large-scale antidunes preserved in deepwater slopes. *Geology*, **47**, 391–394.

Winterwerp, J.C., **Bakker, W.T.**, **Mastbergen, D.R.** and **Van Rossum, H.** (1992) Hyperconcentrated sand-water mixture flows over erodible bed. *J. Hydraul. Eng.*, **118**, 1508–1525.

Wynn, R.B. and **Stow, D.A.V.** (2002) Classification and characterisation of deep-water sediment waves. *Mar. Geol.*, **192**, 7–22.

Wynn, R.B., **Piper, D.J.W.** and **Gee, M.J.R.** (2002) Generation and migration of coarse-grained sediment waves in turbidity current channels and channel-lobe transition zones. *Mar. Geol.*, **192**, 59–78.

Xu, J.P. and **Noble, M.A.** (2009) Variability of the Southern California wave climate and implications for sediment transport. *Geol. Soc. Am. Spec. Pap.*, **454**, 171–191.

Xu, J.P., **Noble, M.A.** and **Rosenfeld, L.K.** (2004) In-situ measurements of velocity structure within turbidity currents. *Geophys. Res. Lett.*, **31**, L09311.

Xu, J.P., **Wong, F.L.**, **Kvitek, R.**, **Smith, D.** and **Paull, C.K.** (2008) Sandwave migration in Monterey Submarine Canyon, central California. *Mar. Geol.*, **248**, 193–212.

Yagishita, K. (1994) Antidunes and traction-carpet deposits in deep-water channel sandstones, Cretaceous, British Columbia, Canada. *J. Sed. Res.*, **A64**, 34–41.

Yang, T., **Cao, Y.** and **Wang, Y.** (2017) A new discovery of the early cretaceous supercritical hyperpycnal flow deposits on Lingshan Island, East China. *Acta Geol. Sinica Engl.*, **91**, 749–750.

Yokokawa, M., **Okuno, K.**, **Kakamura, A.**, **Muto, T.**, **Miyata, Y.** and **Naruse, H.** (2009) Aggradational cyclic steps: sedimentary structures found in flume experiments. Vancouver, Canada. *Proceedings of the 33rd International Association for Hydro-Environment Engineering (IAHR) Congress*, **81**, pp. 5547–5554.

Zhong, G., **Cartigny, M.J.**, **Kuang, Z.** and **Wang, L.** (2015) Cyclic steps along the South Taiwan Shoal and West Penghu submarine canyons on the northeastern continental slope of the South China Sea. *Geol. Soc. Am. Bull.*, **127**, 804–824.

Supporting Information

Additional information may be found in the online version of this article:

Appendix S1. Tables comparing statistics for the absolute magnitude of seafloor change observed in difference maps created between bathymetric surveys. (A) Comparison of seafloor change observed in difference maps that encompass flow events (rows coloured in red) and those with no documented events from the Squamish prodelta dataset. (B) Comparison of seafloor changes observed in difference maps within the active channel and on the canyon flanks from the Monterey Canyon dataset.

Appendix S2. (A) Seafloor difference maps created between surveys encompassing flow events in the Squamish prodelta dataset. (B) Corresponding profiles from along the channel thalweg – location indicated by white-dashed line in (A) – show upslope-migration of bedform crests between survey time steps.

Appendix S3. (A) Seafloor difference maps of the axial channel created between surveys in the Monterey Canyon dataset. (B) Corresponding profiles from along the channel thalweg – location indicated by white-dashed line in (A) – show reworking and migration of bedform crests between survey time steps.

Appendix S4. Videos capturing the stratigraphic evolution observed by stacking repeat-bathymetric profiles to produce the stratigraphic reconstructions in Figs 9A, 10A and 17C. For each time step, red lines represent the profile of the associated bathymetric surface while black lines and filled polygons show preservation of previous surfaces and deposits. Three-dimensional stratigraphic reconstructions from the Squamish prodelta include dip, oblique and strike cross-sectional profiles as well as 3D bathymetric surfaces with 1 m contours for each survey.

Appendix S5. Compiled metrics for bedforms and bedform deposits including wavelength, wave height, deposit thickness and deposit length.